nature microbiology

ANALYSIS

https://doi.org/10.1038/s41564-021-01026-3

Check for updates

Systematic evaluation of horizontal gene transfer between eukaryotes and viruses

Nicholas A. T. Irwin[1,2,3]✉, Alexandros A. Pittis[3], Thomas A. Richards[2] and Patrick J. Keeling[3]

Gene exchange between viruses and their hosts acts as a key facilitator of horizontal gene transfer and is hypothesized to be a major driver of evolutionary change. Our understanding of this process comes primarily from bacteria and phage co-evolution, but the mode and functional importance of gene transfers between eukaryotes and their viruses remain anecdotal. Here we systematically characterized viral–eukaryotic gene exchange across eukaryotic and viral diversity, identifying thousands of transfers and revealing their frequency, taxonomic distribution and projected functions. Eukaryote-derived viral genes, abundant in the *Nucleocytoviricota*, highlighted common strategies for viral host-manipulation, including metabolic reprogramming, proteolytic degradation and extracellular modification. Furthermore, viral-derived eukaryotic genes implicate genetic exchange in the early evolution and diversification of eukaryotes, particularly through viral-derived glycosyltransferases, which have impacted structures as diverse as algal cell walls, trypanosome mitochondria and animal tissues. These findings illuminate the nature of viral–eukaryotic gene exchange and its impact on the evolution of viruses and their eukaryotic hosts.

The exchange of genes between viruses and eukaryotes through horizontal gene transfer (HGT) is a key evolutionary driver capable of facilitating host manipulation and viral resistance[1–4]. Host-derived genes are known to be employed by viruses for replication and cellular control[1,5]. This trend is observed across a diversity of viral lineages that encode cellular-derived informational genes, such as tRNA synthetases and polymerases, as well as operational genes, such as immune effectors and metabolic enzymes[5–12]. These genes counter host immunity, hijack cellular machinery and circumvent nutritional bottlenecks, making them key resources for adaptation[1,13].

Conversely, viral-derived genes in eukaryotic genomes have been frequently perceived as inconsequential remnants of viral interactions[14]. However, these genes can be co-opted, supplementing or supplanting existing cellular components, or providing entirely novel functionality. For example, core proteins such as histones and E2F transcription factors have been replaced by viral proteins in dinoflagellates and fungi, respectively[15,16], while viral structural proteins, fusogens and proviruses are utilized for communication, cellular fusion and antiviral defence in mammals and other eukaryotes[2,3,17–19]. The co-option of such viral proteins has also been found to coincide with cellular innovation and the radiation of major eukaryotic lineages where these genes serve key functions[20,21]. Accordingly, these transfers have important evolutionary, ecological and health implications; nonetheless, we lack a general understanding of the mode, tempo and functional importance of viral–eukaryotic gene exchange, largely due to the absence of standardized analyses across diverse taxa.

Systematic identification of gene transfer events reveals patterns of viral–eukaryotic gene exchange

To reconcile this lack of a systematic survey, we comprehensively characterized viral–eukaryotic gene transfer in 201 eukaryotic and 108,842 viral taxa, covering the diversity of eukaryotic and viral species with genomic representation, by developing a phylogenetic pipeline capable of screening thousands of evolutionary trees for HGT-indicative topologies while accounting for phylogenetic statistics and contamination (Extended Data Figs. 1 and 2). These analyses identified 1,333 candidate (that is, both well- and weakly supported) virus-to-eukaryote transfers, 4,807 eukaryote-to-virus transfers, and 600 transfers with unknown directionality, altogether affecting 2,841 distinct protein families (Fig. 1a and Supplementary Table 1), and including multiple previously characterized examples (such as transporters, signalling proteins, metabolic enzymes and viral housekeeping genes[5,6,9,22–24]). To reduce false positives, phylogenetically ambiguous ($n=607$) or long branching ($n=2,133$) HGTs were considered weakly supported and were excluded in downstream analyses (Fig. 1a, included in Supplementary Table 1). Given our emphasis on specificity over sensitivity, along with limitations in taxon sampling and homology detection, these figures represent a conservative estimate of HGT events.

The resulting HGTs revealed trends regarding the nature of viral–eukaryotic gene exchange. Transfers from eukaryotes to viruses were observed approximately twice as frequently as transfers in the reverse direction (Fig. 1a). This imbalance is explained by the higher number of viral recipients compared with donors per eukaryotic taxon (Fig. 1b) and the greater number of genes transferred to each viral recipient relative to those received per viral donor (Fig. 1c,d). These data also demonstrate a correlation between the number of viral recipients and donors per eukaryote ($r_{Pearson}=0.49$, $P<1\times10^{-18}$, Fig. 1b), suggesting that viral–eukaryotic gene transfer is reciprocal but biased towards viral acquisition. Although sampling bias could influence these numbers, taxon representation affects both recipient and donor frequencies, and bootstrap estimates based on random sampling of protein phylogenies corroborated the observed disparity (Fig. 1a). This bias may reflect the expanded repertoire of eukaryotic genes or differing recombination and fixation rates in eukaryotes and viruses[25,26], all of which could generate greater opportunity for viral gene acquisition during host–pathogen interactions.

Identifying the taxonomy of donors and recipients revealed the propensity of certain lineages to participate in HGT. The vast

[1]Merton College, University of Oxford, Oxford, UK. [2]Department of Zoology, University of Oxford, Oxford, UK. [3]Department of Botany, University of British Columbia, Vancouver, British Columbia, Canada. ✉e-mail: nicholas.irwin@merton.ox.ac.uk

majority of transfers involved double-stranded DNA viruses (97.6%), particularly the nucleocytoplasmic large DNA viruses (NCLDV or *Nucleocytoviricota*, including groups such as the *Phycodnaviridae*, *Mimiviridae*, *Iridoviridae*, *Pithoviridae*, *Asfarviridae* and *Poxviridae*), which were the main contributors to genetic exchange across eukaryotic diversity (82.5%, $n=3{,}109$), consistent with their large and flexible genomes, long and intimate co-evolution with eukaryotes, and wide host breadth (Fig. 1e,f and Extended Data Fig. 1c)[8,27–30]. However, transfers involving alternative lineages such as herpesviruses ($n=47$), baculoviruses (for example, nucleopolyhedroviruses, $n=26$), RNA viruses (predominantly retroviruses, $n=93$) and bacteriophages (for example, *Caudovirales*, $n=67$) were also documented, in accordance with previous observations (Extended Data Figs. 3 and 4, and Supplementary Table 1)[9,31–33]. Among eukaryotes, gene exchange was more prevalent in unicellular compared with multicellular organisms (Fig. 1g), and was particularly abundant in unicellular opisthokonts (the protist relatives of animals and fungi), the diverse protist clade known as SAR (Stramenopila, Alveolata and Rhizaria), and other ecologically important algal groups such as chlorophytes and haptophytes (Fig. 1e,f). This included numerous HGTs coinciding with the diversification of SAR, and the largest influx of viral genes was detected around the origin of the dinoflagellates (Fig. 1e,f and Extended Data Figs. 3 and 4). Elevated gene transfer among unicellular eukaryotes may result from more frequent encounters with NCLDV, which are hyper-diverse and abundant in aquatic environments[8], as well as a lack of germline segregation (Weissman barrier), which probably contributes to the reduced frequency of HGTs observed in animals and plants (Fig. 1f,g)[34]. However, it is important to note that our methodology under-represents retroviral acquisitions, which are commonly observed throughout animal and plant lineages, but whose detection is limited in this analysis by the poor availability of host-free retroviral genome assemblies that are required for phylogenetic interpretation[35].

We also noted eukaryotic species harbouring particularly large numbers of viral genes (Fig. 1c,f). These included species previously described to contain substantial viral genomic insertions from phycodnaviruses (*Ectocarpus siliculosus* and *Tetrabaena socialis*), phycodnaviruses and asfarviruses (*Hyphochytrium catenoides*), or multiple poorly classified viruses (*Acanthamoeba castellanii*), indicating a single or few sources (Fig. 1c,f, Extended Data Fig. 4 and Supplementary Table 1)[24,36–38]. Other species also exhibited elevated numbers of viral genes derived from multiple NCLDV viruses (Fig. 1c,f). Whether these genes retain functional roles, such as in antiviral virophage production[23,39], or reflect remnants of past infections[40,41], is unclear. However, large multigene acquisitions (for example, ten or more genes) were rarely observed at ancestral ($n=1$) relative to terminal nodes ($n=13$), with the exception of the dinoflagellate ancestor (Fig. 1f). This suggests that large-scale transfers, potentially resulting from viral integrations, have recurrently affected diverse eukaryotic lineages, but are generally only transiently retained, possibly providing an opportunity for the longer-term retention and co-option of individual viral genes given adaptive importance.

Along with these transfers to eukaryotes, we identified a number of genes seemingly exchanged before the eukaryotic radiation. These transfers are inherently challenging to interpret given their antiquity, potential rooting uncertainty and ambiguity resulting from intra-eukaryotic HGT[42]. Nonetheless, we observed multiple HGTs probably representing either ancient transfers from NCLDV viruses to early eukaryotic ancestors or recurrent viral acquisitions of eukaryotic genes during eukaryogenesis. These included core informational genes originally derived from Archaea, such as RNA polymerases, DNA topoisomerase I, methionine aminotransferase 2 and replication factor C (RepC), the last of which involves transfers of three RepC subunits, similar to that observed in RNA polymerase (Extended Data Fig. 5a–d)[11]. Furthermore, GDP-L-fucose synthase, which functions in fructose and mannose metabolism, was also involved in an ancient exchange (Extended Data Fig. 5e)[43]. These data suggest that genetic exchange between ancestral eukaryotes and NCLDV viruses may have been important during eukaryogenesis, corroborating earlier observations and hypotheses[11,21,44].

Direction and functional associations of gene transfers

To further investigate the functional relevance of these HGTs, we examined the transfer direction and functional annotations of exchanged protein families. Of the 1,859 families exhibiting HGT with known directionality, the majority (93%) underwent unidirectional transfer (that is, eukaryote-to-virus or virus-to-eukaryote transfer; Fig. 2a). Dividing this dataset by direction, genes involved in eukaryote-to-virus exchanges were generally transferred unidirectionally (92% unidirectional), whereas a larger proportion of families undergoing virus-to-eukaryote transfer participated in bidirectional exchange (71% unidirectional and the remainder exhibiting both eukaryote-to-virus and virus-to-eukaryote transfers; Fig. 2a), suggesting that some of these exchanges may represent transduction (cell-virus-cell HGT). By moving across the phylogenies of all families exhibiting virus-to-eukaryote transfers, from viral donors towards the root, we estimated that 30.5% ($n=259$) of viral genes acquired by eukaryotes were originally eukaryotic, whereas fewer (8.2%, $n=70$) originated in prokaryotes, perhaps reflecting the differential utility or abundance of these genes in eukaryotic and viral systems (Extended Data Fig. 6 and Supplementary Table 1). The remainder had unclear origins (24.2%, $n=205$) or were not attributable to a cellular lineage (37.1%, $n=315$), suggesting that these genes are either viral innovations, ancient viral acquisitions sharing deep cellular homology undetectable in our dataset, or

Fig. 1 | The mode and taxonomic distribution of viral–eukaryotic gene exchange. a, Number of transfers from eukaryotes-to-viruses (E-to-V), viruses-to-eukaryotes (V-to-E), and those with unknown directionality (Unkn.). Recipients and donors were based on the last common ancestor of the recipients and their sister clades. Weakly supported transfers had long branching or ambiguous participants and were excluded from subsequent analyses (see Methods). Error bars represent 95% confidence intervals estimated from bootstrap pseudoreplicates ($n=1{,}000$; random sampling of protein families with replacement). **b**–**d**, Scatterplots comparing gene exchange statistics. Points represent eukaryotic taxa and dashed lines represent lines of equality. **e**,**f**, Gene transfers from E-to-V (**e**) and V-to-E (**f**) across a eukaryotic phylogeny. Bar charts represent HGTs present in an individual genome, whereas pie charts present inferred ancestral HGTs. Bar height and pie diameter reflect transfer frequency and colours denote viral taxonomy. For clarity, viral taxa were mapped to their nearest family, phylum, or higher-level classification. Because of this, multiple families from the same phylum are shown, such as the NCLDV lineages which are denoted with an asterisk (note that some unclassified viruses include candidate NCLDV lineages). Eukaryotic supergroups are labelled with a coloured ring and exemplary taxa are represented using Phylopic images (see http://phylopic.org/). Taxonomic information and phylogenies are based on the NCBI Taxonomy database[92]. Transfers assigned to the last eukaryotic common ancestor are excluded but are listed in Supplementary Table 1. **g**, Boxplots comparing the number of HGTs observed in multicellular and unicellular taxa participating in HGT. The boxes span from the first to the third quartiles, with whiskers extending 1.5 times the interquartile range. Black horizontal lines represent the median and *P* values were calculated using two-sided Welch's *t*-tests (****$P=5.61\times10^{-5}$, ***$P=4.36\times10^{-4}$). Higher-level taxa encompassing both uni- and multicellular organisms were omitted. *H. s.*, *Homo sapiens*; *E. s.*, *Ectocarpus siliculosus*; *T. s.*, *Tetrabaena socialis*; *H. c.*, *Hyphochytrium catenoides*; *A. c.*, *Acanthamoeba castellanii*; *E. h.*, *Emiliania huxleyi*; *G. t.*, *Guillardia theta*; *B. n.*, *Bigelowiella natans*; *N. g.*, *Naegleria gruberi*.

are ambiguous due to taxon sampling deficiencies (Extended Data Fig. 6a). These data demonstrate that over evolutionary time, viruses have a capacity to mediate intra-eukaryotic and inter-domain HGT (that is, transfers between eukaryotes and prokaryotes) through transduction, the relative frequencies of which will be important to assess comprehensively in the future. This provides further evidence that viruses act as a gene conduit between diverse eukaryotic lineages, as suggested previously[45,46], which is reminiscent of prokaryotes where viral transduction is key in ecological adaptation and genome evolution[47,48].

Direction of transfer was also associated with distinct functional biases. Relative to eukaryotic protein families as a whole, eukaryote-to-virus transfers were enriched in functions associated with cellular activity and housekeeping, such as metabolic proteins, E3-ligases and tRNA synthetases (Fig. 2a,b and Supplementary Tables 1 and 3). The enrichment of metabolic proteins implicates cellular-derived genes in reprogramming host metabolism during infection, which appears to be achieved through both de novo metabolite synthesis pathways and uptake (for example, metabolic enzymes and/or nutrient transporters), as well as cellular recycling

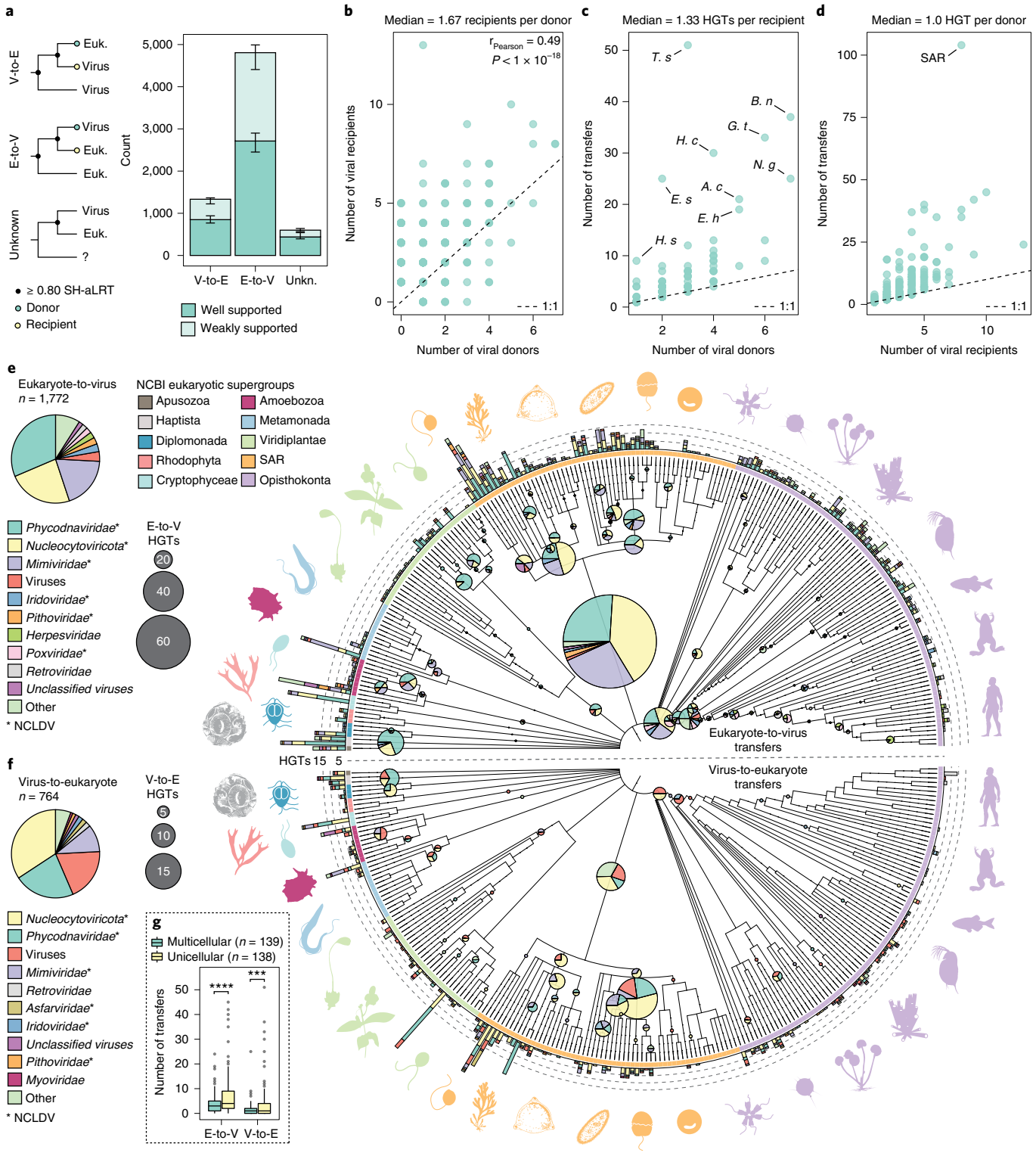

via proteolysis (for example, proteasomal degradation and autophagy) (Fig. 2a,b and Supplementary Tables 1 and 3)[1]. Additionally, signalling and stress response proteins were frequently acquired and probably also contribute to regulating host physiology, gene expression, immune responses and viral assembly[9,49]. The functions of viral-derived genes in eukaryotes were less obvious and have fewer functional associations, but are strongly enriched for proteins functioning in glycosylation ($P < 1 \times 10^{-6}$) and, to a lesser extent, nuclear proteins (Fig. 2a,c and Supplementary Tables 1 and 3). Bidirectionally transferred genes are also enriched in metabolic processes, protein modification and stress response proteins, which represent a subset of functions most often acquired by viruses (Fig. 2d and Supplementary Tables 1 and 3). These data show that eukaryote-to-virus and virus-to-eukaryote HGTs both involve functional tendencies that are not equivalent, but may reflect the different adaptive contexts of viruses and eukaryotes[50].

Eukaryote-derived viral genes are associated with distinct cellular processes and compartments

To understand how these genes are used in viral and eukaryotic systems, we first examined the subcellular targets of eukaryote-derived viral proteins to understand where the proteins may operate in host cells. Cellular localizations were predicted using a neural network-based approach (DeepLoc)[51], revealing that most eukaryote-to-virus HGTs probably function in the cytoplasm ($n = 909$), nucleus ($n = 482$), mitochondrion ($n = 284$) and extracellular space ($n = 214$) (Fig. 3a and Supplementary Table 1). However, relative to all eukaryotic protein families, viral acquisitions were enriched in cytoplasmic, endoplasmic reticulum (ER), extracellular and peroxisomal proteins, the last of which suggests functions involving lipid catabolism and oxidation (Fig. 3b). Moreover, predicted localizations were generally equivalent between donor and recipient proteins, with variation probably resulting from prediction inconsistencies, viral sequence divergence or potentially from neofunctionalization (Fig. 3c, 71% consistent)[51,52]. This indicates that eukaryote-derived gene products tend to function in the same subcellular context as the original host-encoded proteins.

To examine the processes that these genes impact in given cellular compartments, we conducted localization-based functional enrichments revealing the functional breadth and cellular processes associated with eukaryote-derived viral genes. Cytoplasmic proteins were largely involved in translation, metabolism, proteolysis and signalling, whereas nuclear proteins mainly functioned in DNA processing, chromatin organization, cell cycle regulation and protein modification (Fig. 3d,e and Supplementary Tables 1 and 4), in agreement with previous studies[1,5,6,10,53–55]. Endoplasmic reticulum proteins were predominantly associated with lipid metabolism and membrane remodelling (Fig. 3f and Supplementary Table 4). Proteins such as sphingolipid synthesis enzymes contributed to the localization bias, since many function in the ER, were frequently transferred (Supplementary Table 1), and are known to be used by diverse viruses for cellular regulation[13,56,57]. Additionally, ER remodelling is important for generating membrane-enclosed viral factories and for replication[58]. Extracellular proteins acquired by viruses were enriched for functions including carbohydrate metabolism and

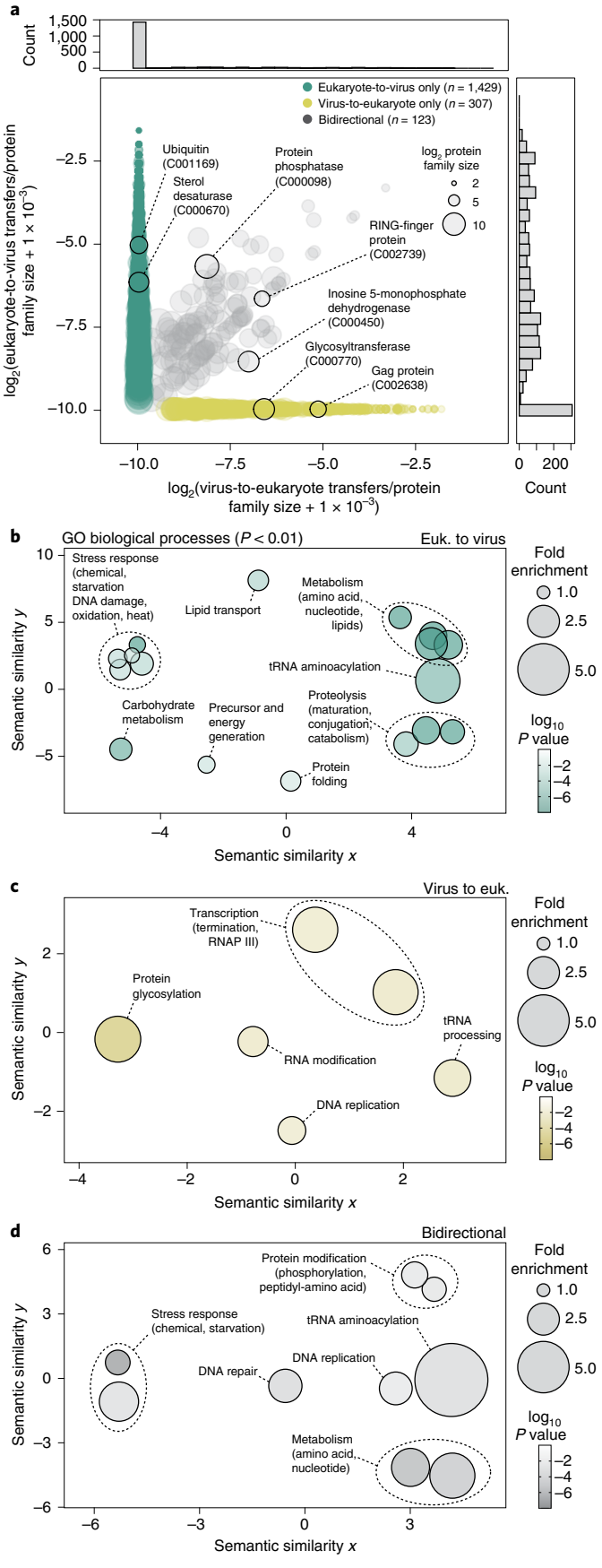

Fig. 2 | Gene function is related to transfer direction. a, A scatterplot relating the frequency of transfer events to protein families, normalized for family size (number of sequences). Individual points represent protein families and functional annotations for exemplary families are highlighted. Histograms denoting point density along the *x* and *y* axes are displayed above and to the right of the scatterplot. **b**–**d**, Scatterplots displaying enriched GO biological process terms from protein families participating in unidirectional (**b**,**c**) and bidirectional transfers (**d**), relative to all eukaryotic protein families. Labelling has been summarized for clarity, but complete terms are available in Supplementary Table 3. Semantic similarity was determined using REVIGO[96] and statistical significance was assessed using two-sided permutation tests ($P < 0.01$, $n = 10^7$).

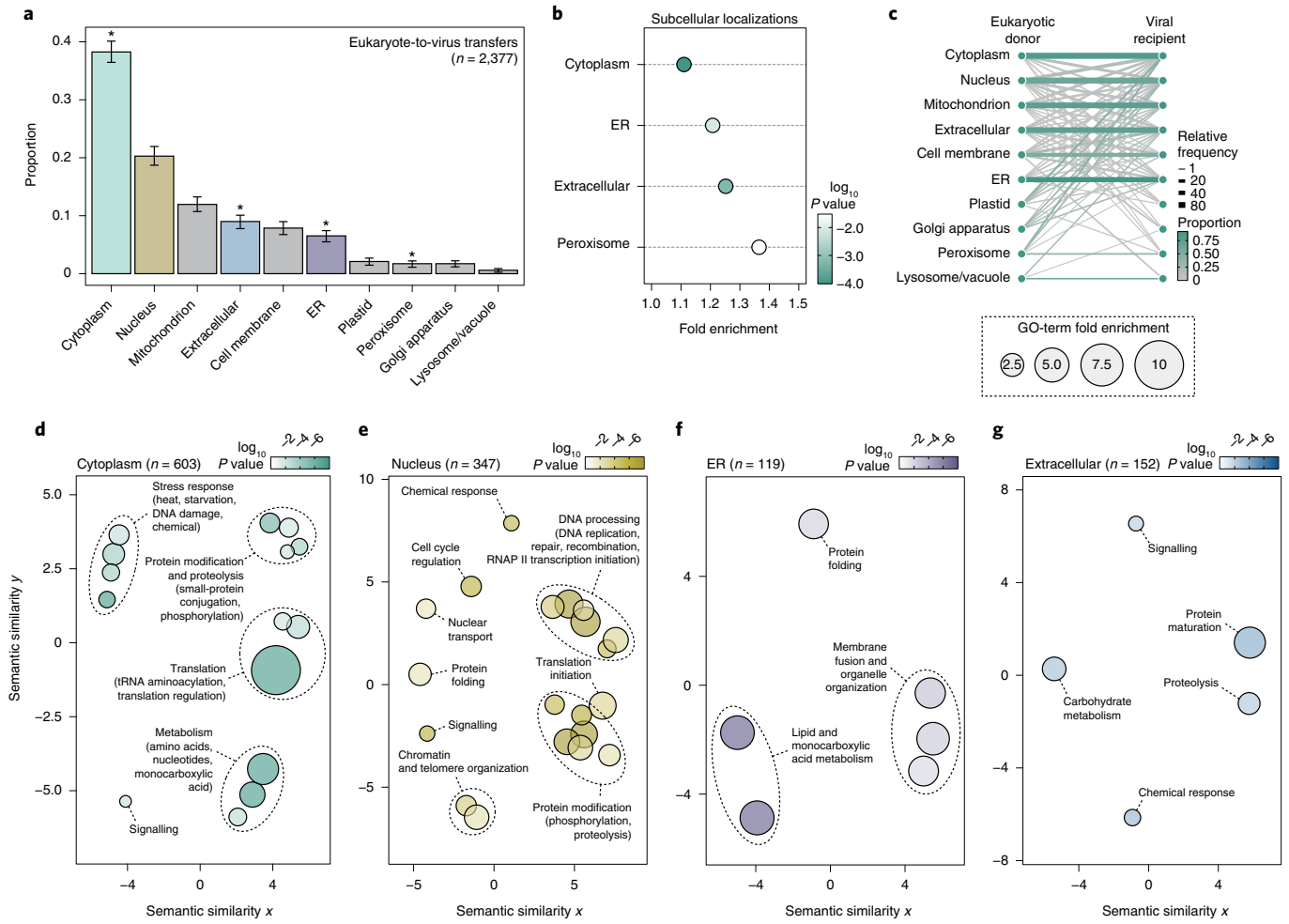

Fig. 3 | Predicted subcellular localizations and functions of eukaryote-derived viral genes. a, Proportions of subcellular localizations for eukaryote-to-virus HGTs based on the predicted targeting of eukaryotic donor sequences. Asterisks denote statistically significant enrichments ($P < 0.05$, see **b**). Error bars represent 95% confidence intervals determined from bootstrap pseudoreplicates ($n = 1{,}000$; random sampling of HGTs with replacement). **b**, Enrichment of subcellular compartments relative to total eukaryotic proteomes. Significance was assessed using two-sided permutation tests ($n = 10^6$). **c**, A comparison between the predicted localization of proteins from eukaryotic donors and their viral recipients. The relative frequencies and proportions are indicated by edge thickness and colour, respectively. **d**–**g**, Scatterplots displaying enriched GO biological process terms for families with a given donor localization relative to all eukaryotic protein families for localizations to (from left to right, colour coded as in **a**) the cytoplasm, nucleus, endoplasmic reticulum and extracellular space. Labelling has been summarized for clarity but complete terms are available in Supplementary Table 4. Semantic similarity was determined using REVIGO and statistical significance was assessed using two-sided permutation tests ($P < 0.01$, $n = 10^7$).

proteolysis, reflecting proteins such as glycosyl hydrolases, glycosyltransferases and S1 peptidases, and implying a tendency for cell-surface alteration (Fig. 3g and Supplementary Table 4). This is consistent with repeated observations of viruses manipulating cell membranes and extracellular spaces through polysaccharide and protein modification[13,59,60]. These results therefore highlight the key cellular systems associated with eukaryote-derived viral genes which, given their known roles in host manipulation[1,6], may provide insights into common viral infection strategies. Indeed, many of these processes are also known to be manipulated by viruses that lack eukaryotic genes (for example, many non-NCLDV viruses), which instead often rely on small effectors and host-encoded proteins[61–63]. This suggests that cellular manipulation strategies may be ubiquitous across viral lineages, but that the mechanism through which modification is accomplished may depend on viral coding capacity (for example, large genome sizes and increased coding capacity in the NCLDV could permit the more flexible use of acquired eukaryotic genes). Notably, the characterization of host–virus interactomes has been proposed as a promising avenue for host-targeting antiviral drug discovery[64,65]. Therefore, if host-manipulation mechanisms are similar across viral lineages, we hypothesize that eukaryote-derived viral genes could facilitate the prediction of cellular components pertinent for infection by diverse viral lineages. Although indirect, this could provide an analytically simplistic (for example, homology-based) approach for predicting therapeutic targets that could complement data from experimental host–virus model systems[65].

The acquisition of viral-derived glycosyltransferases correlates with eukaryotic morphological transitions

Lastly, to gain insights into the role viral genes play in eukaryotic systems, we inspected the distributions and functions of viral-derived glycosyltransferases, which were strongly enriched in the identified virus-to-eukaryote HGTs (Fig. 2c). We identified 63 instances of eukaryotes acquiring viral glycosyltransferases, of which 13 mapped to ancestral nodes, implying functional relevance under long-term selection (Supplementary Table 5). Plotting transfer events and annotations over a eukaryotic phylogeny revealed the functional

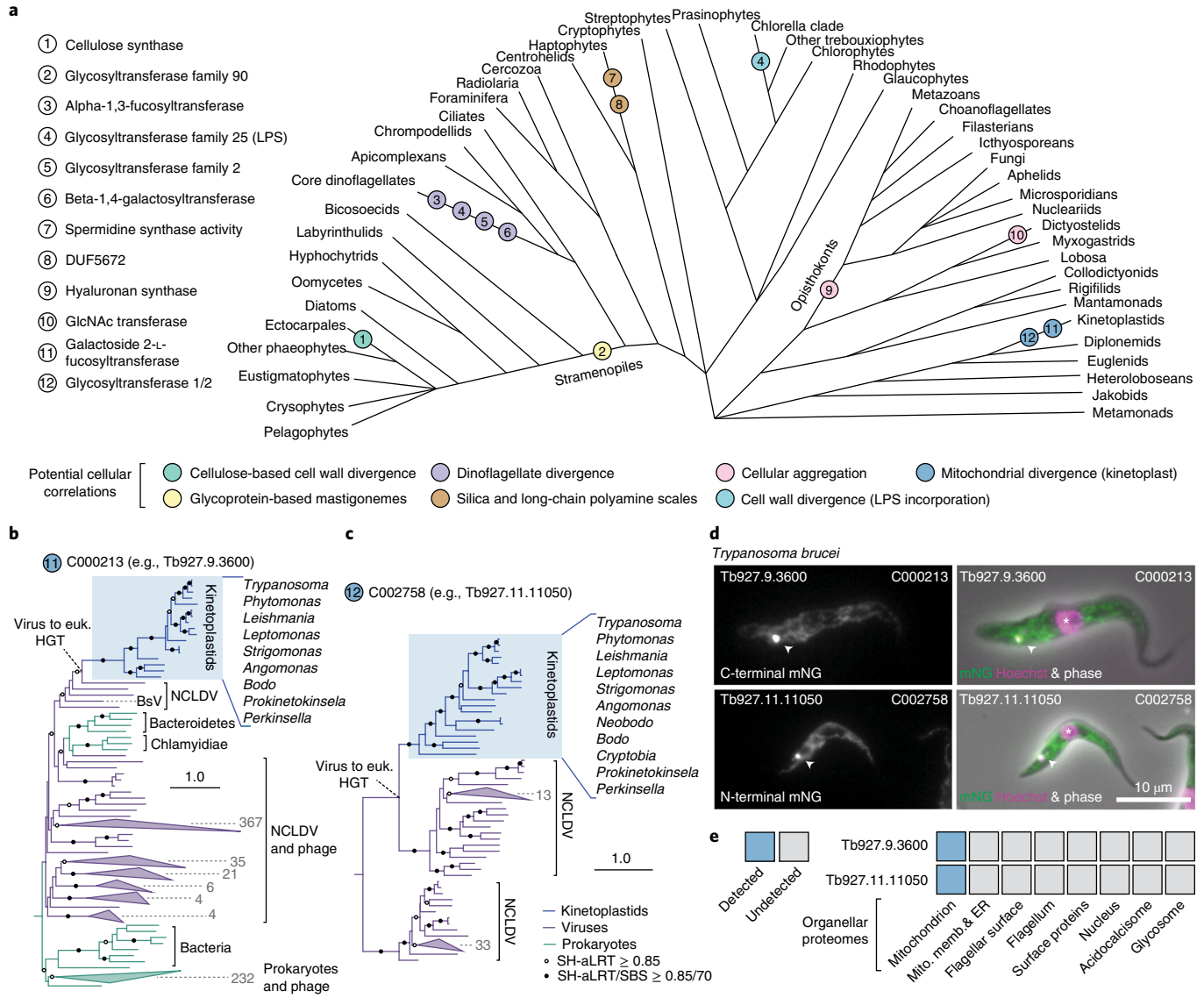

Fig. 4 | Recurrent acquisition of viral glycosyltransferases across the eukaryotic tree of life. a, A schematic eukaryotic phylogeny, based on previous phylogenomic studies[99], with glycosyltransferase acquisitions plotted at ancestral nodes. Protein families and annotations are denoted with numbers and phenotypic correlations are noted with colours. **b**,**c**, The phylogenetic origin of kinetoplastid glycosyltransferases from NCLDV by HGT. Maximum likelihood phylogenies were generated in IQ-Tree using the LG+F+R10 (**b**) and LG+F+R6 (**c**) substitution models as selected using ModelFinder, and statistical support was assessed using SH-aLRT and standard bootstraps (SBS) (n=1,000)[86,88]. Kinetoplastid genera and the gene identifiers for *Trypanosoma brucei* orthologues are noted. **d**, Viral-derived glycosyltransferases function in highly derived kinetoplastid mitochondria (including kinetoplasts). Representative TrypTag fluorescent micrographs, based on observations of at least 20 individual cells, depicting the localization of two glycosyltransferases (Tb927.9.3600 and Tb927.11.11050) after labelling with mNeonGreen (left) and Hoechst DNA stain (right). White arrowheads and asterisks denote kinetoplasts and nuclei, respectively. **e**, Organellar proteomic data displaying the presence or absence of both glycosyltransferases in **d**. Proteomic data were assessed using TriTrypDB.

diversity and recurrent acquisitions of these enzymes across eukaryotic lineages (Fig. 4a and Extended Data Fig. 7). These HGTs were often correlated with morphological and structural synapomorphies, including algal cell wall elaboration (for example, lipopolysaccharide (LPS) and cellulose synthesis enzymes)[66], long-chain polyamine-containing scale formation in haptophytes (spermidine synthase)[67], cellular aggregation in opisthokonts and dictyostelid slime moulds (hyaluronan synthase and GlcNAc transferase), and mitochondrial structural divergence in the kinetoplastids (fucosyltransferase), a group primarily comprised of animal parasites such as trypanosomes (Fig. 4a). Experimental data supported a number of these correlations, including the unusual identification of LPS in the cell walls of *Chlorella*[68], the importance of hyaluronan in vertebrate tissues[69], and the role of the dictyostelid *N*-acetylglucosamine transferase, Gnt2, in calcium-independent cellular aggregation[70], indicating that virally sourced genes are co-opted during the evolution of novel cellular traits (Fig. 4a). We further examined two glycosyltransferase acquisitions in kinetoplastids, hypothesizing that, given the correlation between the HGT acquisitions and the origin of the highly derived kinetoplastid mitochondria (containing kinetoplasts), they should function in that compartment. Phylogenetic analyses revealed that both genes were derived from NCLDV, highlighted the prokaryotic origin of the fucosyltransferase (C000231), and confirmed that both genes are conserved throughout kinetoplastids (Fig. 4b,c). Moreover, both proteins localized to the mitochondria and kinetoplast in

Trypanosoma brucei (identifiable as a non-nuclear DNA-stained foci) both when tagged with mNeonGreen (Fig. 4d) and by organellar proteomics (Fig. 4e). A recent report also suggested an essential role for the fucosyltransferase in mitochondrial function in *T. brucei*[71], altogether indicating that these viral-derived glycosyltransferases were co-opted for use in the kinetoplastid mitochondria as it underwent massive evolutionary change. These data, in combination with the capacity for viruses to modify cell surfaces and induce morphological alterations in their hosts (for example, cytopathic effects)[72], suggest that viral-derived genes may have played various roles in the evolution of cellular morphology across the eukaryotic tree of life.

Discussion

Horizontal gene transfer between viruses and eukaryotes has been observed and assumed to impact the evolution of both participants, but until now we lacked the systematic characterization necessary to generalize the mode and functional importance of these transfers in both viral and eukaryotic contexts[2,29,37]. As with all computational surveys, our dataset is limited by specificity and sensitivity, but nonetheless it provides an extensive resource from which phylogenetic patterns can be observed and their genomic and functional importance may be predicted. From a viral perspective, the preponderance of host-derived genes in the NCLDV reiterates the importance of gene exchange in the evolution of these viruses[27], and underscores the ubiquity of certain viral host-manipulation strategies. Indeed, many important emerging human pathogens, such as Zika and coronaviruses, depend on the manipulation of similar eukaryotic systems, such as autophagy, proteolysis, ER modification and sphingolipid metabolism[57,73,74]. Similarly, functional investigations of eukaryote-derived viral genes, particularly using heterologous expression[6], may also provide insights into how viruses manipulate these cellular pathways while circumventing the need for tractable host–virus model systems. From a eukaryotic perspective, our analyses provide further evidence that viruses participate in eukaryotic transduction and implicate viral–eukaryotic gene exchange in eukaryogenesis and the evolution of eukaryotic morphology. In particular, horizontally acquired glycosyltransferases have recurrently impacted transitions as fundamental as the evolution of tissues and divergence of mitochondria, reminiscent of how retroviral genes, such as fusogens, have repeatedly driven placental evolution in animals[19,75]. Our survey also identified protein candidates for which experimental characterizations could help reveal the impact of these genes on cellular systems and their roles in driving the evolution of eukaryotic complexity.

Methods

Dataset assembly. To systematically and conservatively identify instances of viral–eukaryotic gene exchange, groups of homologous eukaryotic, viral and prokaryotic proteins were clustered into protein families and phylogenetic analyses were performed (Extended Data Fig. 1a). To do this, a eukaryotic dataset was generated from 196 genome-predicted eukaryotic proteomes, primarily from UniProt (release 2018_11), derived from diverse species from all available major eukaryotic supergroups. These proteomes were individually clustered at 99% percent-identity with Cd-hit v4.8.1[76] to reduce redundancy resulting from recent paralogues and isoforms, and combined. The eukaryotic dataset was further supplemented with five complete transcriptomes (four dinoflagellates (MMETSP0224, MMETSP0227, MMETSP0228, MMETSP0790) and a cercozoan (SRR3221671) with over 90% BUSCOs (Benchmarking Universal Single Copy Orthologs) present using the alveolata_odb10 (for the dinoflagellates) or eukaryota_odb10 (for *Paulinella*) databases, assessed using BUSCO v4.1.4) to fill taxonomic gaps in lineages with poor genomic sampling[77,78]. Viral proteins predicted from the genomes of diverse viral taxa, including DNA and RNA viruses, were obtained from UniProt and filtered to exclude those derived from Human Immunodeficiency Virus-1, which were over-represented (Extended Data Fig. 1b,c). Additional viral proteins were acquired from nucleocytoplasmic large DNA virus (NCLDV) metagenomes previously assembled from diverse environments and assessed as having low contamination on the basis of gene content (see Contamination scoring below)[8]. Viral taxonomic annotations were assigned to metagenomes on the basis of previously conducted phylogenomic analyses[8].

Eukaryotic and viral proteins were then clustered into protein families using a similarity-based approach and the Markov clustering (MCL) algorithm (inflation = 2) after comparing sequences to one another using Diamond v2.0.2 BLASTp (sensitive mode, *E*-value < 10^{-5}, query coverage >50%) (Extended Data Fig. 1a, step i)[79,80]. Protein families containing both viral and eukaryotic representatives were retained, aligned with MAFFT v.7.397[81], and used to generate profile hidden Markov models (HMMs), which were used to search 9,035 prokaryotic proteomes from UniProt with HMMER v.3.1b2 (*E*-value < 10^{-5}, incE < 10^{-5}, domE < 10^{-5})[82] (Extended Data Fig. 1a, step i). In this case, HMMs were used to improve the detection of distant prokaryotic homologues. Due to the large number of prokaryotic sequences, the resulting hits were reduced by taking the most significant hit (based on *E*-value) per genus or per strain, to a maximum of 150 sequences; this allowed for diverse taxon sampling while avoiding an overabundance of prokaryotic proteins (Extended Data Fig. 1a, step i). Sequences assigned to viral–eukaryotic protein families were then combined with the prokaryotic proteins and re-clustered as described above (Extended Data Fig. 1a, step ii).

Phylogenetic analysis. Phylogenetic trees were generated from clustered protein families to infer the evolutionary relationships between viral and eukaryotic homologues. Protein families were filtered to retain only those with viruses and eukaryotes, aligned with MAFFT (—auto), trimmed using a gap-threshold of 20% in trimAl v1.2, and sequences with less than 50 amino acid positions were removed (Extended Data Fig. 1a,d,e)[83]. Maximum likelihood phylogenies were conducted in IQ-Tree v1.6 using the robust and generic LG+F+R5 substitution model, and statistical support was calculated using SH-aLRT (Shimodaira–Hasegawa approximate likelihood ratio test, $n = 1{,}000$), which was chosen due to its speed, insensitivity to model violations and taxon sampling, and its comparable conservativeness to standard bootstrapping[84–86]. Phylogenies for large protein families with over 1,500 sequences ($n = 103$) were generated using the fast search mode in IQ-Tree. Phylogenetic rooting was done using minimal ancestral deviation, which is a rooting method that is more robust to heterotachy than midpoint rooting[87].

For individual phylogenies of particular interest, such as those shown in Fig. 4 and Extended Data Figs. 5–7, analyses were repeated as above but after alignment with the more accurate L-INS-i algorithm in MAFFT (or —auto for C000038) and limited curation (for example, the removal of long-branching taxa as defined below, see Horizontal gene transfer detection below). Additionally, substitution models were selected using ModelFinder in IQ-Tree[86,88] and phylogenies were visualized and annotated using iTOL v4[89]. Notably, the topologies of these trees were consistent with their initial iterations and ModelFinder consistently selected the Le and Gascuel (LG) substitution model similar to that used in the other phylogenies, corroborating the use of the aforementioned methods (see Extended Data Figs. 6 and 7). Before phylogenetic inference, the trimmed alignments for protein families inferred to exhibit ancient gene transfers (for example, Extended Data Fig. 5) were recoded using 4-bin Dayhoff recoding to reduce the effects of saturation and compositional heterogeneity, as done previously[11,42,90].

Horizontal gene transfer detection. To detect instances of HGT, we developed a conservative algorithmic approach that emphasized specificity over sensitivity, given the potential for contamination in the underlying dataset and the risk of phylogenetic artefacts. We developed an automated pipeline using the python package, ETE 3[91], to identify HGT-indicative topologies in the phylogenetic trees generated from each protein family. Specifically, we aimed to identify eukaryotic species nested within viral clades (viral-to-eukaryote HGT) or viral taxa within eukaryotic clades (eukaryote-to-virus HGT) (Extended Data Fig. 2a). To this end, phylogenies were initially processed to account for statistical support and directionality (that is, rooting), and to assign taxonomic annotations. First, phylogenetic nodes with SH-aLRT values below 0.8 were collapsed, a threshold with a false positive rate similar to a standard bootstrap support of 60%[84] (Extended Data Fig. 2a, step i). Collapsed phylogenies were then rooted using minimal ancestral deviation rooting[87] and taxa were annotated as eukaryotic, viral or prokaryotic using the National Centre for Biotechnology Information (NCBI) Taxonomy database (Extended Data Fig. 2a, step i)[92]. Viral taxonomic annotations in the NCBI Taxonomy database are in part based on the International Committee on the Taxonomy of Viruses (ICTV) classifications[93].

Following tree processing and annotation, but before identifying HGT events, the phylogenies were analysed to assess rooting ambiguity (Extended Data Fig. 2a, step ii). In particular, we checked whether viral and eukaryotic sequences could be separated into two monophyletic groups using alternative root placements. In this case, rooting becomes unclear unless the phylogeny is strongly biased toward viral or eukaryotic species representation (for example, it is unlikely that a gene conserved throughout a eukaryotic supergroup was derived from a single virus). To evaluate this, if a phylogeny could be split into two discrete taxonomic clades, the ratio of eukaryotic to viral species was determined. If the ratio was heavily skewed towards eukaryotes or viruses (eukaryote:viral species ratio >49 or <0.15, reflecting the top and bottom 20% of all protein families), the tree was rooted normally. Otherwise, the topology would be classified as an HGT with unknown directionality. Lastly, single prokaryotic sequences and HGTs between prokaryotes

and viruses or eukaryotes (identified as described below) were removed to reduce topology complexity, but this did not increase the false positive rate among viral–eukaryotic HGTs (Extended Data Fig. 2a, step ii).

After processing, phylogenies were screened for HGT topologies (Extended Data Fig. 2a, step iii). To achieve this, viral and eukaryotic clades were identified and the taxonomy of their sister group (that is, the most closely related phylogenetic group) and 'cousin' group (that is, the second most closely related phylogenetic group) were determined. A eukaryote-to-virus HGT topology was defined as a viral clade with a eukaryotic sister and cousin whereas a virus-to-eukaryote HGT required a eukaryotic clade with a viral sister and cousin (Extended Data Fig. 2a, step ii). Initially, viral and eukaryotic clades were identified and the taxonomy of their sister and cousin groups were assessed. To classify the taxonomy of these groups, the numbers of viral, eukaryotic and prokaryotic sequences in each group were counted. Sister and cousin groups were then classified as viral, eukaryotic or prokaryotic if the taxonomies were consistent across the members of the group. If the taxonomies of a group were mixed (for example, if both viral and eukaryotic sequences were present), but viral or eukaryotic taxa dominated at least 80% of the sequences, the group was described as 'probably' viral or eukaryotic, or else the group received an ambiguous designation. In the event of a polytomy, multiple sister and cousin groups could be present. To account for this, the taxonomy of the polytomy-wide group would be summarized by determining the taxonomy of each group within the polytomy (as described above). If all candidate sisters or cousins within the polytomy were classified consistently, the group would be identified as viral, eukaryotic or prokaryotic according to the consistent classification. Likewise, if a majority (more than two-thirds) of the groups were consistently classified, the sister or cousin would be denoted as 'probably' viral or eukaryotic, otherwise it would be labelled as ambiguous. After classifying both sister and cousin groups, if the topology was consistent with one of the aforementioned scenarios, an HGT event would be noted (Extended Data Fig. 2a, step iii). Each phylogeny was screened for eukaryote-to-virus and virus-to-eukaryote HGTs three times iteratively, given that once a viral or eukaryotic clade had been classified as an HGT, it would be interpreted as eukaryotic or viral, respectively, in subsequent iterations. Finally, after three cycles of HGT identification, if there were remaining viral and eukaryotic clades sister to one another with ambiguous or prokaryotic cousins, they were labelled as HGTs with unknown transfer directionality.

Once an HGT was identified, characteristics including the recipient, donor, phylogenetic statistics and topology notes were recorded (Extended Data Fig. 2a, step iv; see Supplementary Table 1). Recipient and donor taxa were assessed by determining the last common ancestor of the recipient and donor (sister), respectively, on the basis of the NCBI Taxonomy database[92]. Moreover, node support values were recorded along with the branch length of the recipient (the distance from recipient node or tip to the transfer node). If the branch length of the recipient or donor represented an extreme outlier (defined as the median branch length of the phylogeny after removing identical branch lengths, plus three times the interquartile range), the HGT was highlighted as a potential long-branch attraction (LBA) artefact (Extended Data Fig. 2a, step iv). Additionally, if the donor only had a 'probable' taxonomic classification, ambiguity would also be noted. In both of these cases, HGTs were labelled as weakly supported and excluded in downstream analyses. Lastly, the approximate origin of viral-derived eukaryotic genes was determined by moving up through phylogenetic nodes from the donor clade towards the root until a cellular lineage was reached, if possible (Extended Data Fig. 3a). The effect of gene sampling on the number of HGTs was assessed using 95% bootstrap confidence intervals, calculated by randomly sampling gene families with replacement to an equal number of families as the original dataset ($n = 1{,}000$) (Fig. 1a).

Contamination scoring. After identifying the HGTs, individual transfer events were assessed for possible alternative sources of phylogenetic incongruence, specifically contamination. This is important since eukaryotic and viral genes can be artefactually present in viral and eukaryotic genomes, respectively, which may give the impression that HGT has occurred. To address this, only viral reference proteomes and metagenomes with low contamination scores (estimated previously on the basis of the representation of core NCLDV genes in a given metagenome relative to those observed in viruses from a related superclade; for more information, see ref. [8]) were included in the analysis and individual viral-derived eukaryotic genes were assessed on the basis of a series of criteria and a contamination scoring scheme (Extended Data Fig. 2b–e). Contamination was assessed on the basis of two main attributes: (1) the presence of related taxa in the HGT, and (2) the characteristics of the genomic contig upon which the gene was encoded. First, the taxonomic composition of the HGT recipients was assessed on the basis of the assumption that the same contamination is unlikely to occur in multiple independently sampled genomic datasets, particularly if the species from which they are derived are closely related. Therefore, points were given if the HGT recipients included multiple members of the same (+3) or different (+1) phyla as the species encoding the gene of interest, on the basis of NCBI Taxonomy (Extended Data Fig. 2b, step i).

Second, the characteristics of the genomic contigs encoding each viral-derived gene were inspected on the basis of the notion that they should share attributes with the host genome, such as consistent GC content, reasonable contig size and that the gene should be flanked by eukaryotic regions. Accordingly, contigs were identified by mapping proteins to the genome using tBLASTn (E-value $< 10^{-5}$) and points were given if the contig was within one standard deviation of the median genomic GC content (+1) and if the contig was a reasonable size (greater than half of the scaffold N50) (+1) (Extended Data Fig. 2b(steps ii–iv),c). Lastly, the genomic context was inspected by extracting DNA regions (5 kbp) upstream (−2.5 kbp) and downstream (+2.5 kbp) of each gene. Extracted regions were then taxonomically classified by comparing them to the SWISS-PROT database (release 2019_11) using BLASTx and assessing the taxonomy of the resulting hits. A maximum of 20 hits (E-value $< 10^{-3}$) were evaluated and normalized scores for viral, eukaryotic and prokaryotic classifications were calculated to account for database bias. These scores were calculated for each taxonomic group as:

$$\text{score}_t = -\log_{10}\left(t_{prop}\right) \times S_t \times n_t$$

where t_{prop} is the proportion of a taxonomic group in the database, and n_t and S_t are the number and median bit-score of hits to that taxonomic group, respectively. The taxonomy was assigned to the group with the maximum score and points were given for eukaryotic classifications (+1 per region) and subtracted for prokaryotic ones (−1 per region), which are more indicative of contamination. Viral and uncertain classifications were neutral (+0) to account for the possibility of large viral insertions (Extended Data Fig. 2b, steps v–vi).

After assigning contamination scores to each putative eukaryotic sequence involved in a virus-to-eukaryote HGT or an HGT with unknown directionality, sequences with scores less than two were excluded and HGTs and recipient taxonomies were reassessed (Extended Data Fig. 2b,d,e). Due to the strict criteria applied during filtering and HGT identification, false positive rates should be low; however, transfers associated exclusively with transcriptomic data should be interpreted with care as these sequences are more challenging to assess (for example, transfers to *Alexandrium*, *Protoceratium*, *Togulla*, *Polarella* and *Paulinella*).

Functional analyses. To examine HGT function, eukaryotic and viral proteins were annotated with eggNOG, PANTHER (protein analysis through evolutionary relationships) and Pfam using a combination of eggNOG-Mapper v2, InterProScan v.5.48 and HMMER v3.1b2 (E-value $< 10^{-3}$) with the default parameters[82,94,95]. For clarity, the resulting gene ontology (GO) terms were simplified by mapping the terms to the yeast GO-slim subset using Map2Slim (see https://github.com/owlcollab/owltools/wiki/Map2Slim). Protein families were given functional annotations on the basis of a majority rule (Supplementary Table 1) and labelled with GO terms if a given term was assigned to at least 20% of annotated proteins within a family. Similarly, Pfam domains were assigned to a given family if they were detected in 20% of annotated proteins. Ultimately, of the 2,841 protein families exhibiting HGT, 2,747 (98.3%) received an annotation, while those that did not tended to be small and divergent (median number of sequences, 9; range, 3–60). To conduct GO-enrichment analyses, we tested the null hypothesis that GO terms associated with the HGTs reflect a random sampling of eukaryotic protein families. To this end, protein families exhibiting HGT were compared against a eukaryotic background comprising all eukaryotic protein families containing either a virus or at least ten eukaryotic species, generated during both MCL clustering steps. The frequencies of individual GO terms in the HGT families were compared to the eukaryotic background using permutation tests that involved randomly sampling equally sized sets of annotated protein families without replacement ($n = 10^7$). Significantly enriched GO terms ($P < 0.01$) were summarized and visualized using REVIGO[96].

To investigate the predicted subcellular localizations of eukaryote-derived viral genes, all eukaryotic proteins were annotated using DeepLoc v1.0 and the BLOSSUM62 matrix[51]. Localization predictions with likelihoods less than 0.5 were re-classified as unknown and cellular targets were assigned to individual eukaryote-to-virus HGTs on the basis of the majority localization of the donor (that is, eukaryotic) sequences. Eukaryotic donor sequences were used for localization characterizations since DeepLoc is trained and optimized using eukaryote encoded proteins[51]. When shown, predictions of eukaryote-derived viral proteins are displayed in the context of their donor sequence localizations. Enrichments were assessed by comparing the frequency of individual localizations in the HGTs to an equally sized random sampling of annotated eukaryotic proteins ($P < 0.05$, $n = 10^6$). The null hypothesis was that viruses randomly acquire eukaryotic genes irrespective of their predicted subcellular localizations. Bootstrap confidence intervals were calculated on the basis of bootstrap resampling of HGT donors ($n = 1{,}000$). Subcellular localizations for *Trypanosoma brucei* proteins were assessed using fluorescent localization and organellar proteomic data obtained from TrypTag and TriTrypDB, respectively[97,98].

Reporting Summary. Further information on research design is available in the Nature Research Reporting Summary linked to this article.

Data availability

All data, including proteomes, protein families, annotations, alignments, phylogenies and summaries of detected HGTs (both before and after

contamination filtering) are available from Dryad (https://datadryad.org/stash/dataset/doi:10.5061/dryad.z08kprrc9).

Code availability

All the code used for phylogenetic interpretation, contamination scoring, and functional enrichments and analyses are available from Dryad (https://datadryad.org/stash/dataset/doi:10.5061/dryad.z08kprrc9).

Received: 24 April 2021; Accepted: 12 November 2021;
Published online: 31 December 2021

References

1. Zimmerman, A. E. et al. Metabolic and biogeochemical consequences of viral infection in aquatic ecosystems. *Nat. Rev. Microbiol.* **18**, 21–34 (2019).
2. Koonin, E. V. & Krupovic, M. The depths of virus exaptation. *Curr. Opin. Virol.* **31**, 1–8 (2018).
3. Frank, J. A. & Feschotte, C. Co-option of endogenous viral sequences for host cell function. *Curr. Opin. Virol.* **25**, 81–89 (2017).
4. Moreira, D. & Brochier-Armanet, C. Giant viruses, giant chimeras: the multiple evolutionary histories of Mimivirus genes. *BMC Evol. Biol.* **8**, 12 (2008).
5. Filée, J., Pouget, N. & Chandler, M. Phylogenetic evidence for extensive lateral acquisition of cellular genes by Nucleocytoplasmic large DNA viruses. *BMC Evol. Biol.* **8**, 320 (2008).
6. Monier, A. et al. Host-derived viral transporter protein for nitrogen uptake in infected marine phytoplankton. *Proc. Natl Acad. Sci. USA* **114**, E7489–E7498 (2017).
7. Monier, A. et al. Horizontal gene transfer of an entire metabolic pathway between a eukaryotic alga and its DNA virus. *Genome Res.* 1441–1449 (2009).https://doi.org/10.1101/gr.091686.109
8. Schulz, F. et al. Giant virus diversity and host interactions through global metagenomics. *Nature* **578**, 432–436 (2020).
9. Aswad, A. & Katzourakis, A. Cell-derived viral genes evolve under stronger purifying selection in rhadinoviruses. *J. Virol.* **92**, e00539-18 (2018).
10. Schulz, F. et al. Giant viruses with an expanded complement of translation system components. *Science* **356**, 82–85 (2017).
11. Guglielmini, J., Woo, A. C., Krupovic, M., Forterre, P. & Gaia, M. Diversification of giant and large eukaryotic dsDNA viruses predated the origin of modern eukaryotes. *Proc. Natl Acad. Sci. USA* **116**, 19585–19592 (2019).
12. Enav, H., Mandel-Gutfreund, Y. & Béjà, O. Comparative metagenomic analyses reveal viral-induced shifts of host metabolism towards nucleotide biosynthesis. *Microbiome* **2**, 9 (2014).
13. Vardi, A. et al. Host-virus dynamics and subcellular controls of cell fate in a natural coccolithophore population. *Proc. Natl Acad. Sci. USA* **109**, 19327–19332 (2012).
14. Biémont, C. A brief history of the status of transposable elements: from junk DNA to major players in evolution. *Genetics* **186**, 1085–1093 (2010).
15. Gornik, S. G. et al. Loss of nucleosomal DNA condensation coincides with appearance of a novel nuclear protein in dinoflagellates. *Curr. Biol.* **22**, 2303–2312 (2012).
16. Medina, E. M., Turner, J. J., Gordân, R., Skotheim, J. M. & Buchler, N. E. Punctuated evolution and transitional hybrid network in an ancestral cell cycle of fungi. *Elife* **5**, e09492 (2016).
17. Pastuzyn, E. D. et al. The neuronal gene Arc encodes a repurposed retrotransposon Gag protein that mediates intercellular RNA transfer. *Cell* **172**, 275–288 (2018).
18. Mi, S. et al. Syncytin is a captive retroviral envelope protein involved in human placental morphogenesis. *Nature* **403**, 785–789 (2002).
19. Cornelis, G. et al. An endogenous retroviral envelope syncytin and its cognate receptor identified in the viviparous placental *Mabuya* lizard. *Proc. Natl Acad. Sci. USA* **114**, E10991–E11000 (2017).
20. Irwin, N. A. T. et al. Viral proteins as a potential driver of histone depletion in dinoflagellates. *Nat. Commun.* **9**, 1535 (2018).
21. Forterre, P. & Prangishvili, D. The major role of viruses in cellular evolution: facts and hypotheses. *Curr. Opin. Virol.* **3**, 558–565 (2013).
22. Delaroque, N., Maier, L., Knippers, R. & Müller, D. G. Persistent virus integration into the genome of its algal host, *Ectocarpus siliculosus* (Phaeophyceae). *J. Gen. Virol.* **80**, 1367–1370 (1999).
23. Blanc, G., Gallot-Lavallée, L. & Maumus, F. Provirophages in the *Bigelowiella* genome bear testimony to past encounters with giant viruses. *Proc. Natl Acad. Sci. USA* **112**, E5318–E5326 (2015).
24. Leonard, G. et al. Comparative genomic analysis of the 'pseudofungus' *Hyphochytrium catenoides*. *Open Biol.* **8**, 170184 (2018).
25. McCrone, J. T. & Lauring, A. S. Genetic bottlenecks in intraspecies virus transmission. *Curr. Opin. Virol.* **28**, 20–25 (2018).
26. Awadalla, P. The evolutionary genomics of pathogen recombination. *Nat. Rev. Genet.* **4**, 50–60 (2003).
27. Koonin, E. V. & Yutin, N. Origin and evolution of eukaryotic large nucleo-cytoplasmic DNA viruses. *Intervirology* **53**, 284–292 (2010).
28. Koonin, E. V., Dolja, V. V. & Krupovic, M. Origins and evolution of viruses of eukaryotes: the ultimate modularity. *Virology* **479–480**, 2–25 (2015).
29. Filée, J. & Chandler, M. Gene exchange and the origin of giant viruses. *Intervirology* **53**, 354–361 (2010).
30. Sun, T.-W. et al. Host range and coding potential of eukaryotic giant viruses. *Viruses* **12**, 1337 (2020).
31. Fraser, M. J., Smith, G. E. & Summers, M. D. Acquisition of host cell DNA sequences by Baculoviruses: relationship between host DNA insertions and FP mutants of *Autographa californica* and *Galleria mellonella* nuclear polyhedrosis viruses. *J. Virol.* **47**, 287–300 (1983).
32. Liu, H. et al. Widespread horizontal gene transfer from double-stranded RNA viruses to eukaryotic nuclear genomes. *J. Virol.* **84**, 11876–11887 (2010).
33. Bordenstein, S. R. & Bordenstein, S. R. Eukaryotic association module in phage WO genomes from *Wolbachia*. *Nat. Commun.* **7**, 13155 (2016).
34. Richards, T. A., Hirt, R. P., Williams, B. A. P. & Embley, T. M. Horizontal gene transfer and the evolution of parasitic Protozoa. *Protist* **154**, 17–32 (2003).
35. Hayward, A., Cornwallis, C. K. & Jern, P. Pan-vertebrate comparative genomics unmasks retrovirus macroevolution. *Proc. Natl Acad. Sci. USA* **112**, 464–469 (2015).
36. Cock, J. M. et al. The *Ectocarpus* genome and the independent evolution of multicellularity in brown algae. *Nature* **465**, 617–621 (2010).
37. Moniruzzaman, M., Weinheimer, A. R., Martinez-Gutierrez, C. A. & Aylward, F. O. Widespread endogenization of giant viruses shapes genomes of green algae. *Nature* **588**, 141–145 (2020).
38. Maumus, F. & Blanc, G. Study of gene trafficking between *Acanthamoeba* and giant viruses suggests an undiscovered family of amoeba-infecting viruses. *Genome Biol. Evol.* **8**, 3351–3363 (2016).
39. Fischer, M. G. & Hackl, T. Host genome integration and giant virus-induced reactivation of the virophage mavirus. *Nature* **540**, 288–291 (2016).
40. Maumus, F., Epert, A., Nogué, F. & Blanc, G. Plant genomes enclose footprints of past infections by giant virus relatives. *Nat. Commun.* **5**, 4268 (2014).
41. Patel, M. R., Emerman, M. & Malik, H. S. Paleovirology – ghosts and gifts of viruses past. *Curr. Opin. Virol.* **1**, 304–309 (2011).
42. Williams, T. A., Embley, T. M. & Heinz, E. Informational gene phylogenies do not support a fourth domain of life for nucleocytoplasmic large DNA viruses. *PLoS ONE* **6**, e21080 (2011).
43. Tonetti, M., Sturla, L., Bisso, A., Benatti, U. & de Flora, A. Synthesis of GDP-L-fucose by the human FX protein. *J. Biol. Chem.* **271**, 27274–27279 (1996).
44. Forterre, P., Gribaldo, S., Gadelle, D. & Serre, M. C. Origin and evolution of DNA topoisomerases. *Biochimie* **89**, 427–446 (2007).
45. Malik, S. S., Azem-e-Zahra, S., Kim, K. M., Caetano-Anollés, G. & Nasir, A. Do viruses exchange genes across superkingdoms of life? *Front. Microbiol.* **8**, 2110 (2017).
46. Gilbert, C. & Cordaux, R. Viruses as vectors of horizontal transfer of genetic material in eukaryotes. *Curr. Opin. Virol.* **25**, 16–22 (2017).
47. Chen, J. et al. Genome hypermobility by lateral transduction. *Science* **362**, 207–212 (2018).
48. Touchon, M., Moura de Sousa, J. A. & Rocha, E. P. Embracing the enemy: the diversification of microbial gene repertoires by phage-mediated horizontal gene transfer. *Curr. Opin. Microbiol.* **38**, 66–73 (2017).
49. Krupovic, M. & Koonin, E. V. Multiple origins of viral capsid proteins from cellular ancestors. *Proc. Natl Acad. Sci. USA* **114**, E2401–E2410 (2017).
50. Moreira, D. & López-García, P. Ten reasons to exclude viruses from the tree of life. *Nat. Rev. Microbiol.* **7**, 306–311 (2009).
51. Almagro Armenteros, J. J., Sønderby, C. K., Sønderby, S. K., Nielsen, H. & Winther, O. DeepLoc: prediction of protein subcellular localization using deep learning. *Bioinformatics* **33**, 3387–3395 (2017).
52. Duffy, S., Shackelton, L. A. & Holmes, E. C. Rates of evolutionary change in viruses: patterns and determinants. *Nat. Rev. Genet.* **9**, 267–276 (2008).
53. Jung, J. U., Stäger, M. & Desrosiers, R. C. Virus-encoded cyclin. *Mol. Cell. Biol.* **14**, 7235–7244 (1994).
54. Erives, A. J. Phylogenetic analysis of the core histone doublet and DNA topo II genes of Marseilleviridae: evidence of proto-eukaryotic provenance. *Epigenetics Chromatin* **10**, 55 (2017).
55. Schvarcz, C. R. & Steward, G. F. A giant virus infecting green algae encodes key fermentation genes. *Virology* **518**, 423–433 (2018).
56. Pagarete, A., Allen, M. J., Wilson, W. H., Kimmance, S. A. & De Vargas, C. Host-virus shift of the sphingolipid pathway along an *Emiliania huxleyi* bloom: survival of the fattest. *Environ. Microbiol.* **11**, 2840–2848 (2009).
57. Schneider-Schaulies, J. & Schneider-Schaulies, S. Sphingolipids in viral infection. *Biol. Chem.* **396**, 585–595 (2015).
58. Fernández de Castro, I., Tenorio, R. & Risco, C. Virus assembly factories in a lipid world. *Curr. Opin. Virol.* **18**, 20–26 (2016).

59. Hiramatsu, S., Ishihara, M., Fujie, M. & Usami, S. Expression of a chitinase gene and lysis of the host cell wall during *Chlorella* virus CVK2 infection. *Virology* **260**, 308–315 (1999).
60. Klenk, H. D. & Garten, W. Host cell proteases controlling virus pathogenicity. *Trends Microbiol.* **2**, 39–43 (1994).
61. Thaker, S. K., Ch'ng, J. & Christofk, H. R. Viral hijacking of cellular metabolism. *BMC Biol.* **17**, 59 (2019).
62. Mahalingam, S., Meanger, J., Foster, P. S. & Lidbury, B. A. The viral manipulation of the host cellular and immune environments to enhance propagation and survival: a focus on RNA viruses. *J. Leukoc. Biol.* **72**, 429–439 (2002).
63. Ravindran, M. S., Bagchi, P., Cunningham, C. N. & Tsai, B. Opportunistic intruders: how viruses orchestrate ER functions to infect cells. *Nat. Rev. Microbiol.* **14**, 407–420 (2016).
64. de Chassey, B., Meyniel-Schicklin, L., Vonderscher, J., André, P. & Lotteau, V. Virus–host interactomics: new insights and opportunities for antiviral drug discovery. *Genome Med.* **6**, 115 (2014).
65. Puschnik, A. S., Majzoub, K., Ooi, Y. S. & Carette, J. E. A CRISPR toolbox to study virus–host interactions. *Nat. Rev. Microbiol.* **15**, 351–364 (2017).
66. Michel, G., Tonon, T., Scornet, D., Cock, J. M. & Kloareg, B. Central and storage carbon metabolism of the brown alga *Ectocarpus siliculosus*: insights into the origin and evolution of storage carbohydrates in eukaryotes. *New Phytol.* **188**, 67–81 (2010).
67. Durak, G. M. et al. A role for diatom-like silicon transporters in calcifying coccolithophores. *Nat. Commun.* **7**, 10543 (2016).
68. Armstrong, P. B., Armstrong, M. T., Pardy, R. L., Child, A. & Wainwright, N. Immunohistochemical demonstration of a lipopolysaccharide in the cell wall of a eukaryote, the green alga, *Chlorella*. *Biol. Bull.* **203**, 203–204 (2002).
69. Laurent, T. C. & Fraser, J. R. E. Hyaluronan. *FASEB* **6**, 2397–2404 (1992).
70. Loomis, W. F., Wheeler, S. A., Springer, W. R. & Barondes, S. H. Adhesion mutants of *Dictyostelium discoideum* lacking the saccharide determinant recognized by two adhesion-blocking monoclonal antibodies. *Dev. Biol.* **109**, 111–117 (1985).
71. Bandini, G. et al. An essential, kinetoplastid-specific GDP-Fuc: β-D-Gal α-1,2- fucosyltransferase is located in the mitochondrion of *Trypanosoma brucei*. *eLife* **10**, e70272 (2021).
72. Schrom, M. & Bablanian, R. Altered cellular morphology resulting from cytocidal virus infection. *Arch. Virol.* **70**, 173–187 (1981).
73. Raaben, M. et al. The ubiquitin-proteasome system plays an important role during various stages of the coronavirus infection cycle. *J. Virol.* **84**, 7869–7879 (2010).
74. Leier, H. C. et al. A global lipid map defines a network essential for Zika virus replication. *Nat. Commun.* **11**, 3652 (2020).
75. Chuong, E. B. The placenta goes viral: retroviruses control gene expression in pregnancy. *PLoS Biol.* **16**, e3000028 (2018).
76. Li, W. & Godzik, A. Cd-hit: a fast program for clustering and comparing large sets of protein or nucleotide sequences. *Bioinformatics* **22**, 1658–1659 (2006).
77. Keeling, P. J. et al. The Marine Microbial Eukaryote Transcriptome Sequencing Project (MMETSP): illuminating the functional diversity of eukaryotic life in the oceans through transcriptome sequencing. *PLoS Biol.* **12**, e1001889 (2014).
78. Simão, F. A., Waterhouse, R. M., Ioannidis, P., Kriventseva, E. V. & Zdobnov, E. M. BUSCO: assessing genome assembly and annotation completeness with single-copy orthologs. *Bioinformatics* **31**, 3210–3212 (2015).
79. Enright, A. J., van Dongen, S. & Ouzounis, C. A. An efficient algorithm for large-scale detection of protein families. *Nucleic Acids Res.* **30**, 1575–1584 (2002).
80. Buchfink, B., Xie, C. & Huson, D. H. Fast and sensitive protein alignment using DIAMOND. *Nat. Methods* **12**, 59–60 (2014).
81. Katoh, K. & Standley, D. M. MAFFT multiple sequence alignment software version 7: improvements in performance and usability. *Mol. Biol. Evol.* **30**, 772–780 (2013).
82. Mistry, J., Finn, R. D., Eddy, S. R., Bateman, A. & Punta, M. Challenges in homology search: HMMER3 and convergent evolution of coiled-coil regions. *Nucleic Acids Res.* **41**, e121 (2013).
83. Capella-Gutiérrez, S., Silla-Martínez, J. M. & Gabaldón, T. trimAl: a tool for automated alignment trimming in large-scale phylogenetic analyses. *Bioinformatics* **25**, 1972–1973 (2009).
84. Anisimova, M., Gil, M., Dufayard, J. F., Dessimoz, C. & Gascuel, O. Survey of branch support methods demonstrates accuracy, power, and robustness of fast likelihood-based approximation schemes. *Syst. Biol.* **60**, 685–699 (2011).
85. Shimodaira, H. & Hasegawa, M. Multiple comparisons of log-likelihoods with applications to phylogenetic inference. *Mol. Biol. Evol.* **16**, 1114–1116 (1999).
86. Nguyen, L. T., Schmidt, H. A., Von Haeseler, A. & Minh, B. Q. IQ-TREE: a fast and effective stochastic algorithm for estimating maximum-likelihood phylogenies. *Mol. Biol. Evol.* **32**, 268–274 (2015).
87. Tria, F. D. K., Landan, G. & Dagan, T. Phylogenetic rooting using minimal ancestor deviation. *Nat. Ecol. Evol.* **1**, 0193 (2017).
88. Kalyaanamoorthy, S., Minh, B. Q., Wong, T. K. F., von Haeseler, A. & Jermiin, L. S. ModelFinder: fast model selection for accurate phylogenetic estimates. *Nat. Methods* **14**, 587–589 (2017).
89. Letunic, I. & Bork, P. Interactive Tree of Life (iTOL) v4: recent updates and new developments. *Nucleic Acids Res.* **47**, 256–259 (2019).
90. Susko, E. & Roger, A. J. On reduced amino acid alphabets for phylogenetic inference. *Mol. Biol. Evol.* **24**, 2139–2150 (2007).
91. Huerta-Cepas, J., Serra, F. & Bork, P. ETE 3: reconstruction, analysis, and visualization of phylogenomic data. *Mol. Biol. Evol.* **33**, 1635–1638 (2016).
92. Federhen, S. The NCBI Taxonomy database. *Nucleic Acids Res.* **40**, 136–143 (2012).
93. Walker, P. J. et al. Changes to virus taxonomy and to the international code of virus classification and nomenclature ratified by the international committee on taxonomy of viruses (2021). *Arch. Virol.* **166**, 2633–2648 (2021).
94. Huerta-Cepas, J. et al. Fast genome-wide functional annotation through orthology assignment by eggNOG-Mapper. *Mol. Biol. Evol.* **34**, 2115–2122 (2017).
95. Jones, P. et al. InterProScan 5: genome-scale protein function classification. *Bioinformatics* **30**, 1236–1240 (2014).
96. Supek, F., Bošnjak, M., Škunca, N. & Šmuc, T. REVIGO summarizes and visualizes long lists of gene ontology terms. *PLoS ONE* **6**, e21800 (2011).
97. Dean, S., Sunter, J. D. & Wheeler, R. J. TrypTag.org: a trypanosome genome-wide protein localisation resource. *Trends Parasitol.* **33**, 80–82 (2017).
98. Aslett, M. et al. TriTrypDB: a functional genomic resource for the Trypanosomatidae. *Nucleic Acids Res.* **38**, 457–462 (2009).
99. Burki, F., Roger, A. J., Brown, M. W. & Simpson, A. G. B. The new tree of eukaryotes. *Trends Ecol. Evol.* **35**, 43–55 (2020).

Acknowledgements

We thank R. Wheeler for providing fluorescent micrographs of *Trypanosoma brucei* as part of TrypTag. This work was supported by grants from the Natural Sciences and Engineering Research Council of Canada (NSERC, RGPIN-2014-03994) and from the Gordon and Betty Moore Foundation (https://doi.org/10.37807/GBMF9201) to P.J.K. N.A.T.I. was supported by a Junior Research Fellowship from Merton College, Oxford and an NSERC Canadian Graduate Scholarship. A.A.P. was supported by a European Molecular Biology Organization (EMBO) Long-term Fellowship (ALTF 118-2017). T.A.R. is supported by a Royal Society University Research Fellowship (UF130382).

Author contributions

N.A.T.I. and A.A.P. conceptualized the project; P.J.K. and T.A.R. acquired funding; N.A.T.I. and A.A.P. conducted the investigations; P.J.K. and T.A.R. provided resources and supervised the project; N.A.T.I. wrote the paper with input from all authors.

Competing interests

The authors declare no competing interests.

Additional information

Extended data is available for this paper at https://doi.org/10.1038/s41564-021-01026-3.

Supplementary information The online version contains supplementary material available at https://doi.org/10.1038/s41564-021-01026-3.

Correspondence and requests for materials should be addressed to Nicholas A. T. Irwin.

Peer review information *Nature Microbiology* thanks Valerian Dolja, Jolien van Hooff and the other, anonymous, reviewer(s) for their contribution to the peer review of this work.

Reprints and permissions information is available at www.nature.com/reprints.

Publisher's note Springer Nature remains neutral with regard to jurisdictional claims in published maps and institutional affiliations.

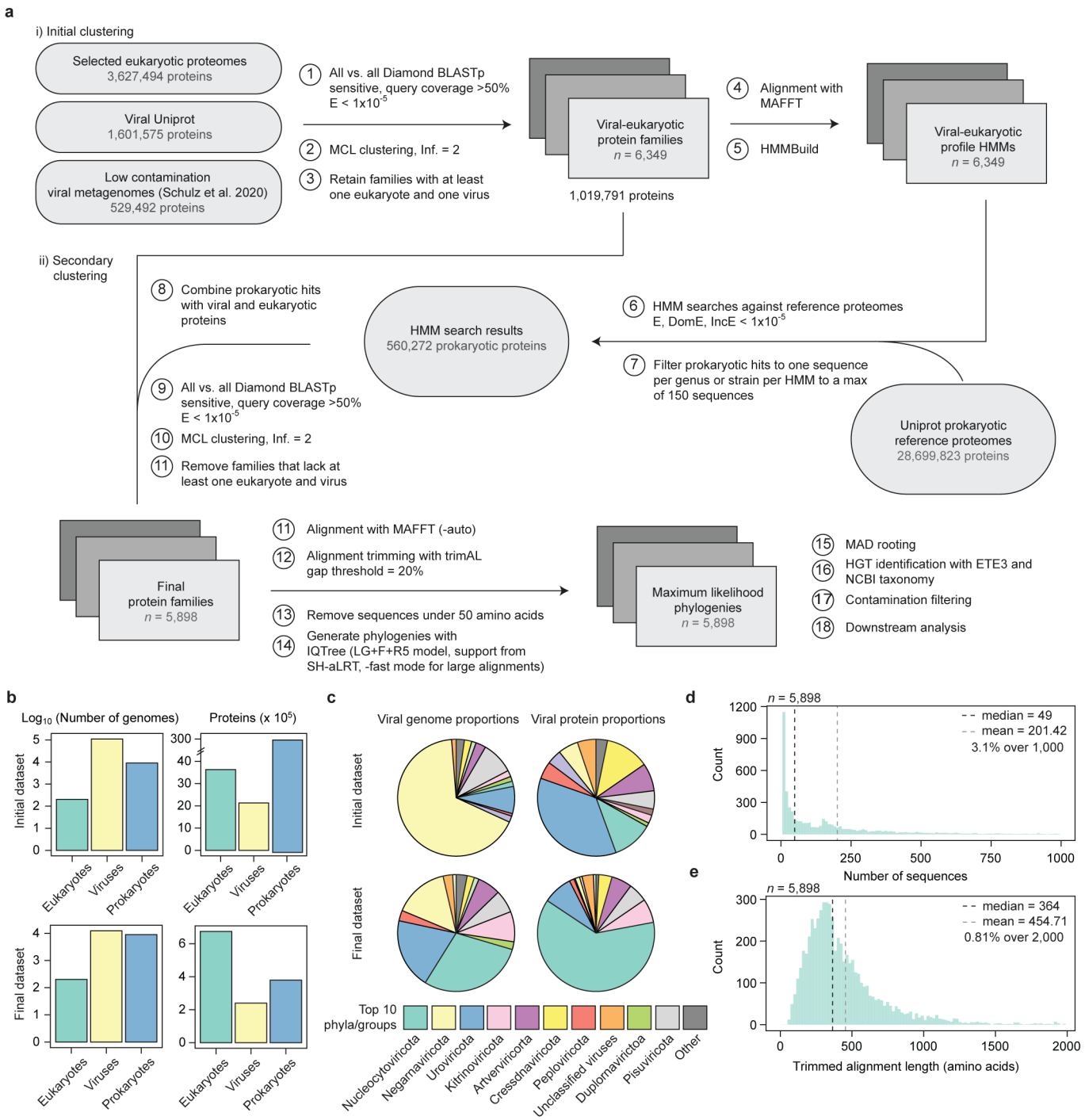

Extended Data Fig. 1 | Dataset assembly and statistics. a. A schematic representation of the dataset assembly pipeline. **b**. The numbers of eukaryotic, viral, and prokaryotic genomes and proteins examined and included in the initial and final dataset. The final dataset reflects the dataset upon which the HGT analysis was conducted. **c**. The representation of viral phyla and other groups (that is, those lacking phyla classifications) in the initial and final datasets. **d, e**. Summary statistics for the final clustered protein families including the number of sequences present (**d**) and the trimmed alignment lengths (**e**). See Methods for additional information.

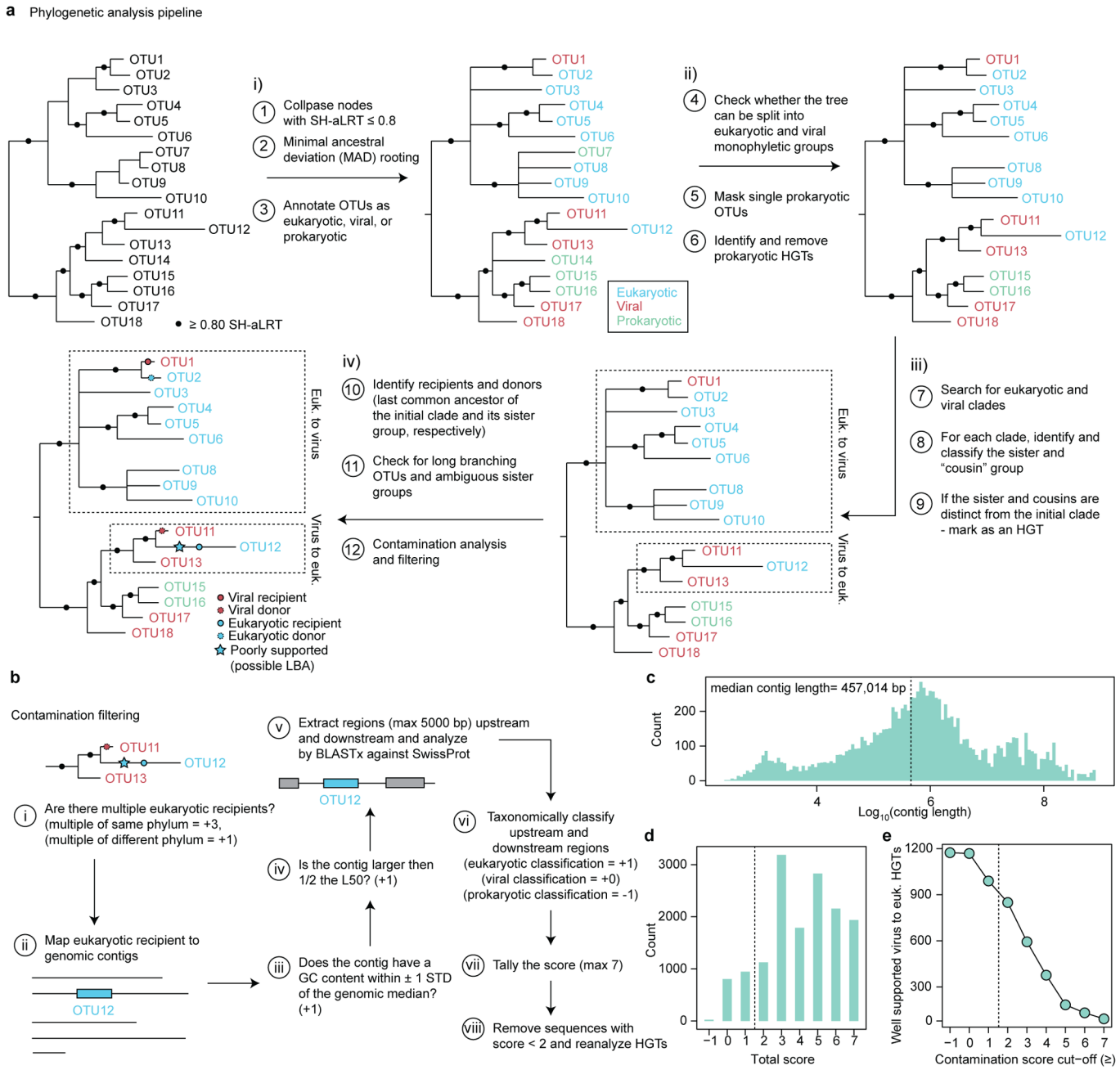

Extended Data Fig. 2 | Phylogenetic pipeline and contamination analysis overview. a, b. Schematic representation of the HGT identification and phylogenetic analysis pipeline (**a**) and the contamination scoring protocol (**b**). **c**. The distribution of eukaryotic contig lengths that contain viral HGTs. **d**. The distribution of contamination scores across eukaryotic recipient sequences. **e**. The number of well-supported HGTs that are identified using different contamination score thresholds. Dashed lines denote the defined scoring threshold (≥ 2). See Methods for additional information.

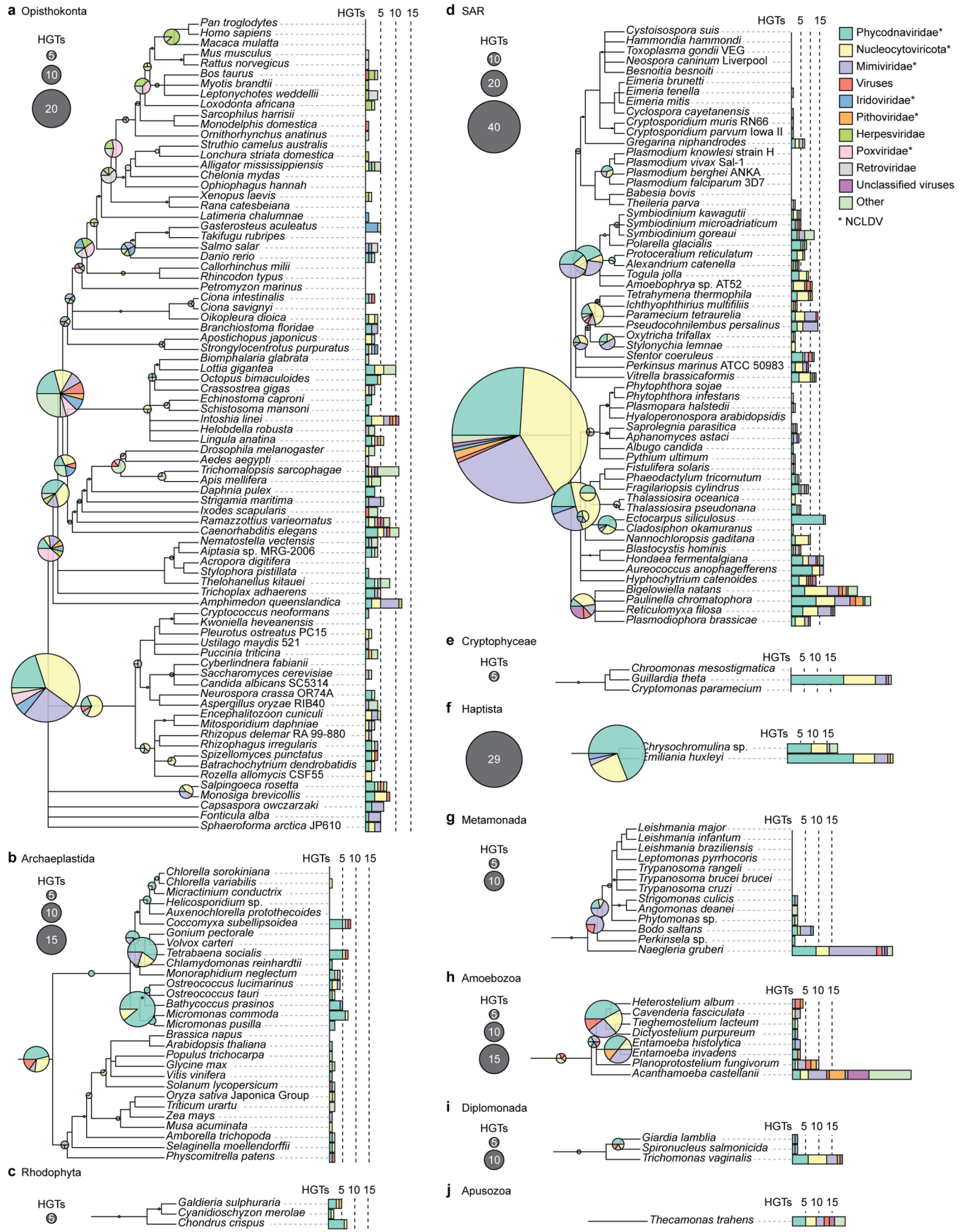

Extended Data Fig. 3 | See next page for caption.

Extended Data Fig. 3 | Eukaryote-to-virus transfers across eukaryotic supergroups. a-j. Expanded versions of Fig. 1e displaying transfers in the Opisthokonta (**a**), Archaeplastida (**b**), Rhodophyta (**c**), SAR (**d**), Cryptophyceae (**e**), Haptista (**f**), Metamonada (**g**), Amoebozoa (**h**), Diplomonada (**i**), and Apusozoa (**j**). Bar charts represent HGTs present in an individual genome, whereas pie charts present inferred ancestral HGTs. Bar height and pie diameter reflect transfer frequency and colours denote viral taxonomy. For clarity, viral taxa were mapped to their nearest family, phylum, or higher-level classification. Because of this, multiple families from the same phylum are shown, such as the NCLDV lineages, which are denoted with an asterisk (note that some unclassified viruses include candidate NCLDV lineages without formal taxonomic descriptions). Taxonomic information and phylogenies are based on the NCBI (National Center for Biotechnology Information) Taxonomy database[92].

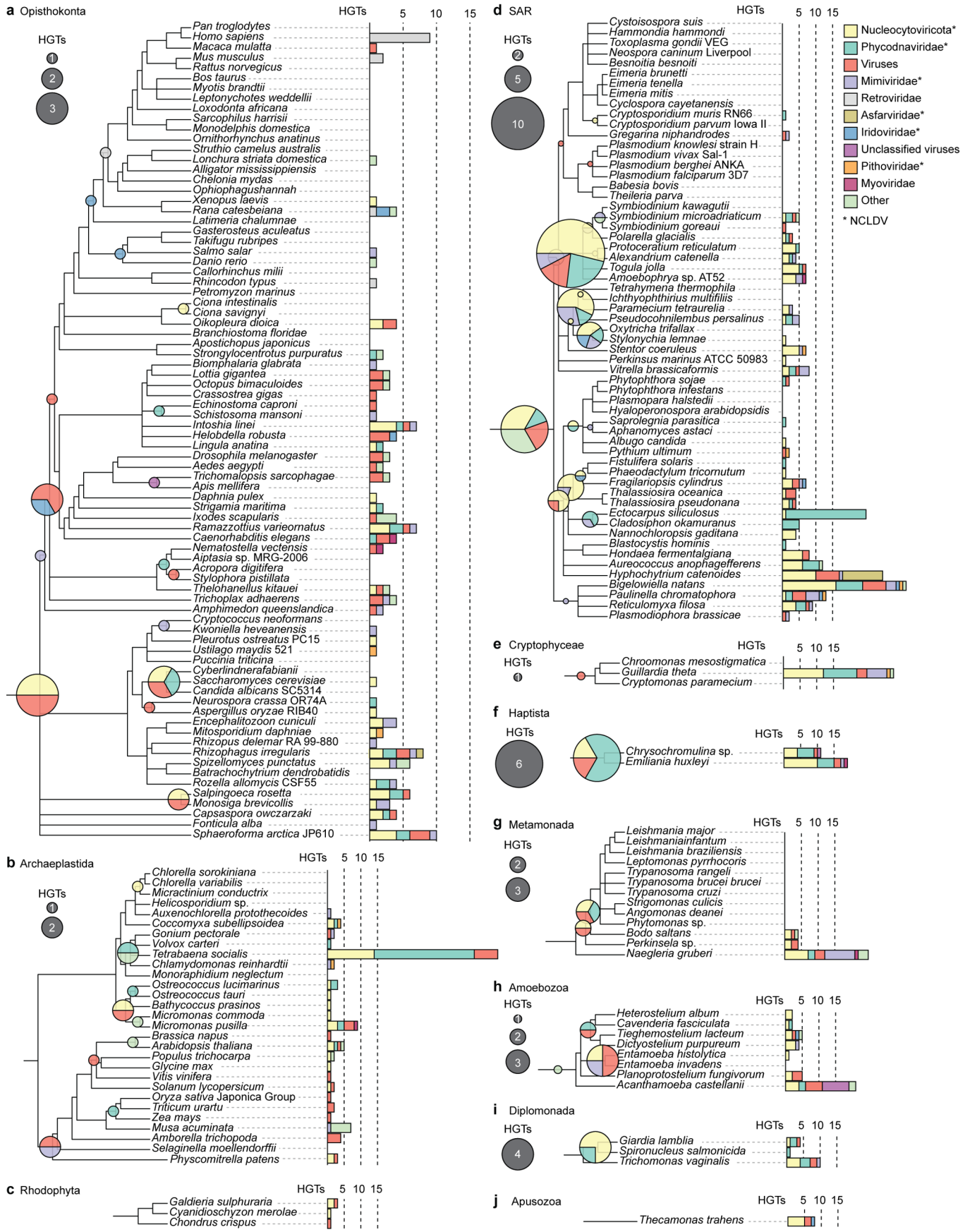

Extended Data Fig. 4 | See next page for caption.

Extended Data Fig. 4 | Virus-to-eukaryote transfers across eukaryotic supergroups. a-j. Expanded versions of Fig. 1f displaying transfers in the Opisthokonta (**a**), Archaeplastida (**b**), Rhodophyta (**c**), SAR (**d**), Cryptophyceae (**e**), Haptista (**f**), Metamonada (**g**), Amoebozoa (**h**), Diplomonada (**i**), and Apusozoa (**j**). Bar charts represent HGTs present in an individual genome, whereas pie charts present inferred ancestral HGTs. Bar height and pie diameter reflect transfer frequency and colours denote viral taxonomy. For clarity, viral taxa were mapped to their nearest family, phylum, or higher-level classification. Because of this, multiple families from the same phylum are shown, such as the NCLDV lineages, which are denoted with an asterisk (note that some unclassified viruses include candidate NCLDV lineages without formal taxonomic descriptions). Taxonomic information and phylogenies are based on the NCBI (National Center for Biotechnology Information) Taxonomy database[92].

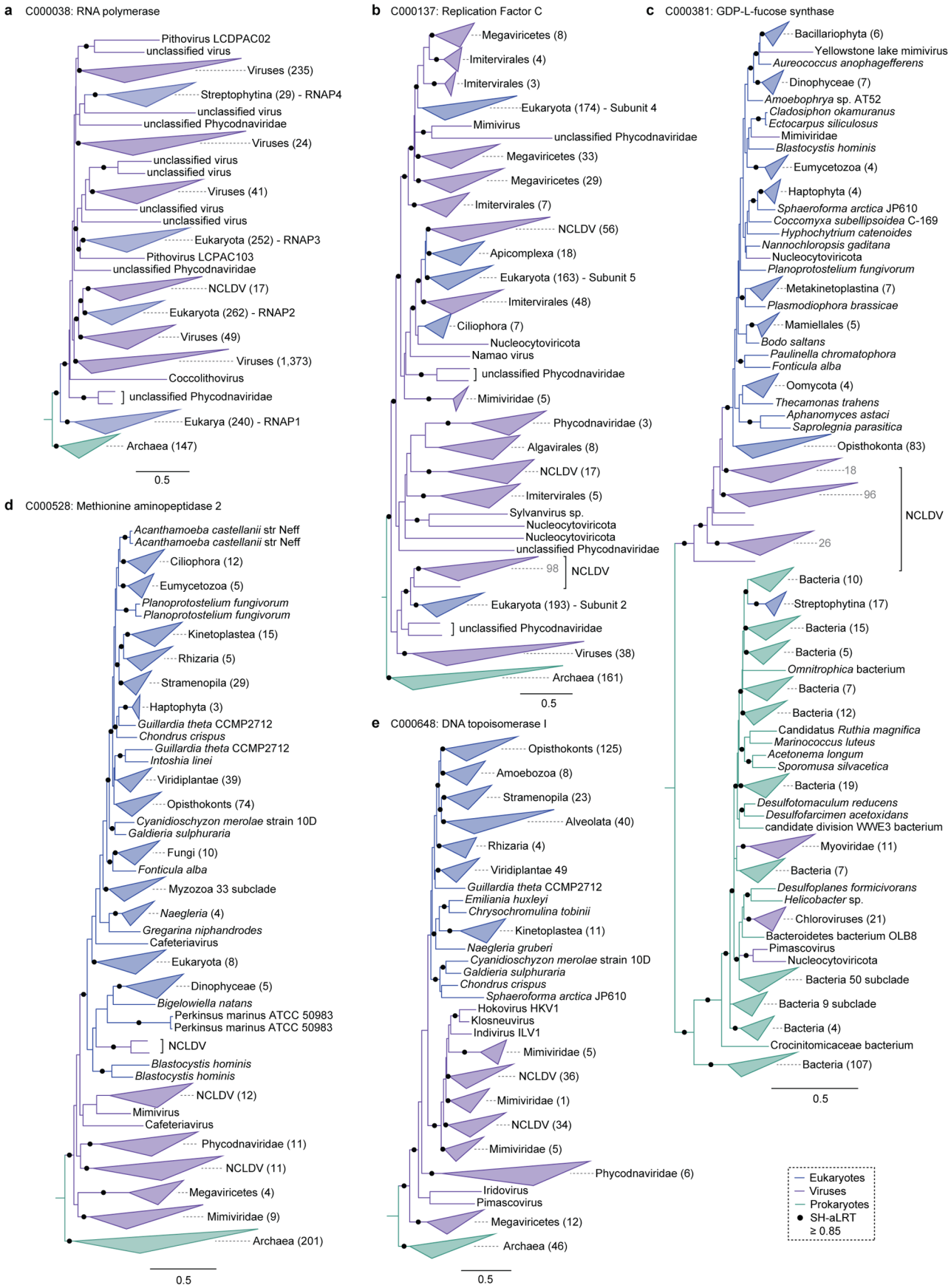

Extended Data Fig. 5 | See next page for caption.

Extended Data Fig. 5 | Examples of ancient viral-eukaryotic gene transfers occurring prior to the last eukaryotic common ancestor. Phylogenetic analyses were conducted in IQ-Tree after recoding alignments with a 4-bin Dayhoff matrix. The number of sequences within collapsed clades are noted and more recent HGTs were removed for clarity but did not affect the tree topologies. Statistical support was assessed using SH-aLRT (n=1,000) and substitution models were selected using ModelFinder and included GTR+F+ASC+R10 (**a**), GTR+F+R10 (**b**), GTR+F+R7 (**c**), GTR+F+R8 (**d**), and GTR+F+R8 (**e**).

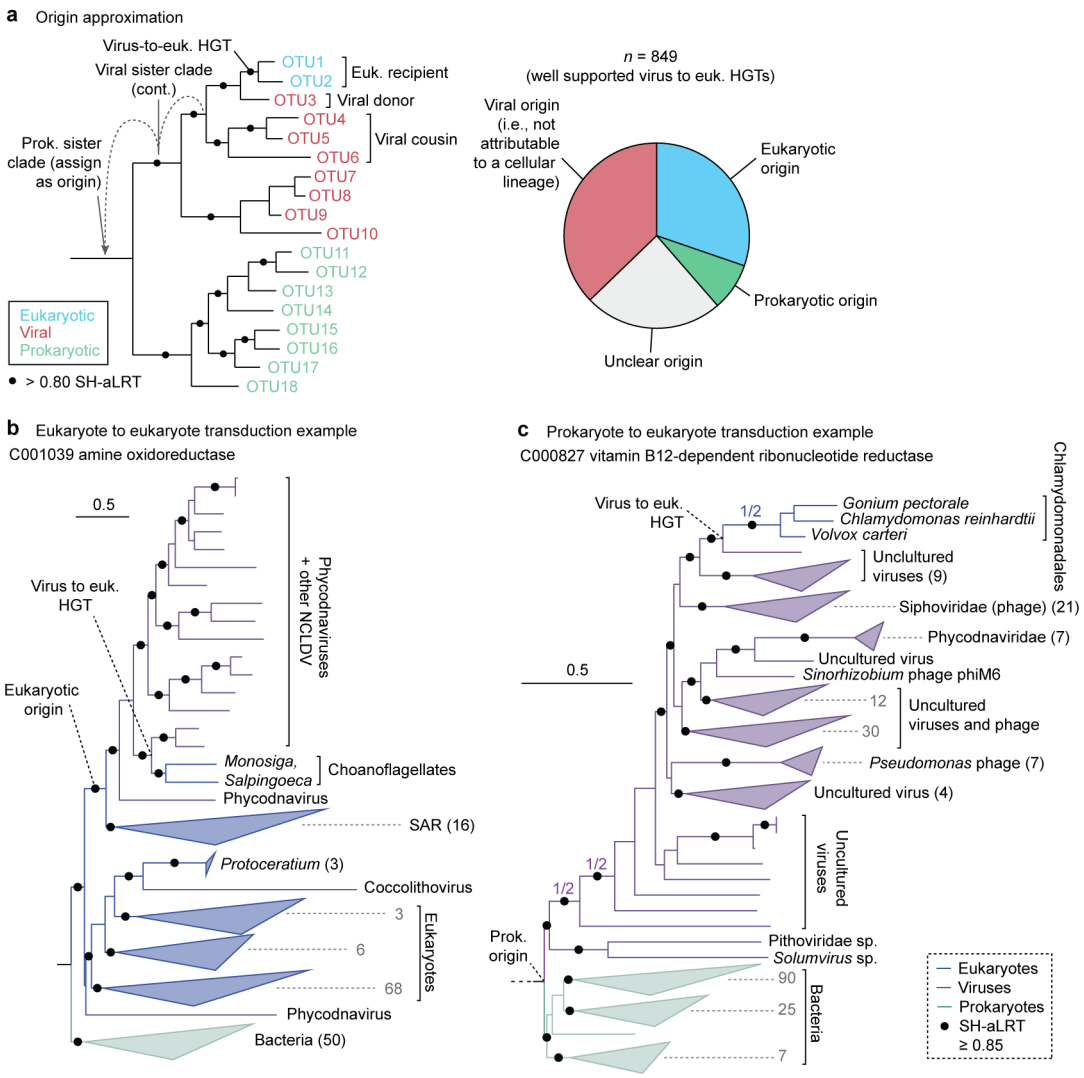

Extended Data Fig. 6 | Gene origin identification and transduction examples. a. A schematic illustrating how viral gene origins were approximated by moving up through the phylogeny from the donor towards the root until a cellular lineage was encountered. The pie chart reflects the proportion of well supported virus-to-eukaryote HGTs that were assigned a given origin. **b, c**. Example phylogenies illustrating cases of eukaryote-to-eukaryote and prokaryote-to-eukaryote transduction. The number of sequences within collapsed clades are noted. Phylogenies were generated in IQ-Tree using the LG+R7 (**b**) or LG+R9 (**c**) substitution models as selected using ModelFinder and statistical support was assessed using SH-aLRT (n=1,000)[86,88].

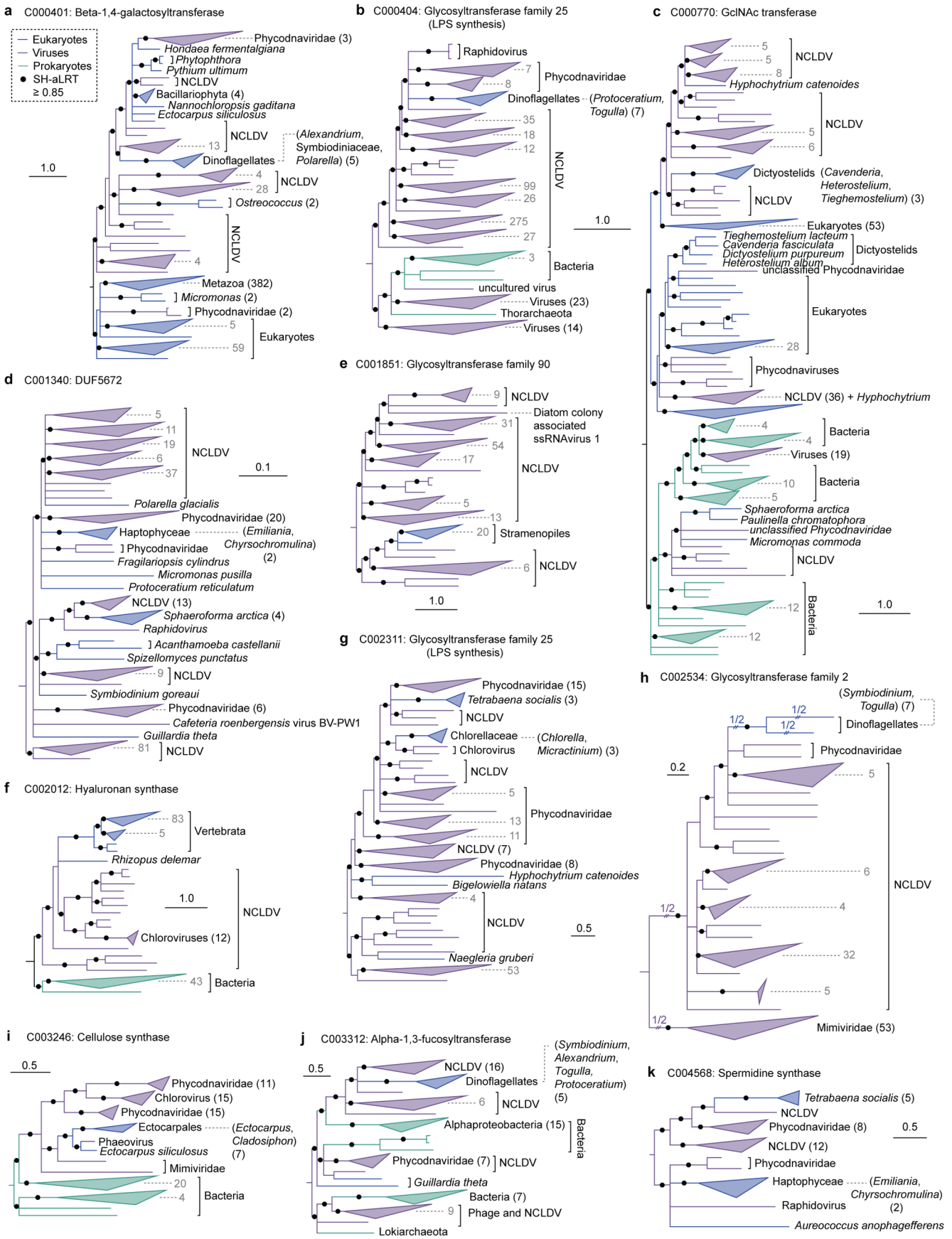

Extended Data Fig. 7 | See next page for caption.

Extended Data Fig. 7 | Phylogenies for glycosyltransferases denoted in Fig. 4. Phylogenetic analyses were conducted in IQ-Tree with statistical support assessed using SH-aLRT ($n = 1{,}000$). The number of sequences within collapsed clades are noted. Substitution models were selected using ModelFinder and included LG+R10 (**a**), LG+F+R10 (**b**), LG+R9 (**c**), LG+F+R8 (**d, e**), LG+R6 (**f**), LG+F+R7 (**g**), LG+F+G4 (**h**), LG+F+R5 (**i, j**), and LG+I+G4 (**k**).

nature portfolio

Corresponding author(s): Nicholas Irwin

Last updated by author(s): Nov 3, 2021

Reporting Summary

Nature Portfolio wishes to improve the reproducibility of the work that we publish. This form provides structure for consistency and transparency in reporting. For further information on Nature Portfolio policies, see our Editorial Policies and the Editorial Policy Checklist.

Statistics

For all statistical analyses, confirm that the following items are present in the figure legend, table legend, main text, or Methods section.

n/a	Confirmed
☐	☒ The exact sample size (*n*) for each experimental group/condition, given as a discrete number and unit of measurement
☒	☐ A statement on whether measurements were taken from distinct samples or whether the same sample was measured repeatedly
☐	☒ The statistical test(s) used AND whether they are one- or two-sided *Only common tests should be described solely by name; describe more complex techniques in the Methods section.*
☒	☐ A description of all covariates tested
☒	☐ A description of any assumptions or corrections, such as tests of normality and adjustment for multiple comparisons
☐	☒ A full description of the statistical parameters including central tendency (e.g. means) or other basic estimates (e.g. regression coefficient) AND variation (e.g. standard deviation) or associated estimates of uncertainty (e.g. confidence intervals)
☐	☒ For null hypothesis testing, the test statistic (e.g. *F*, *t*, *r*) with confidence intervals, effect sizes, degrees of freedom and *P* value noted *Give P values as exact values whenever suitable.*
☒	☐ For Bayesian analysis, information on the choice of priors and Markov chain Monte Carlo settings
☒	☐ For hierarchical and complex designs, identification of the appropriate level for tests and full reporting of outcomes
☒	☐ Estimates of effect sizes (e.g. Cohen's *d*, Pearson's *r*), indicating how they were calculated

Our web collection on statistics for biologists contains articles on many of the points above.

Software and code

Policy information about availability of computer code

Data collection	No software was used for data collection.
Data analysis	All analyses were conducted using freely available software or custom code written in Python 3. The software used includes Diamond v2.0.2, Cd-hit v4.8.1, BUSCO v4.1.4, MAFFT v7.397, HMMER v3.1b2, trimAl v1.2, IQ-Tree v1.6, iTOL v4, ModelFinder, ETE3, eggNOG-Mapper v2, InterProScan v5.48, Map2Slim, and DeepLoc v1.0. All custom code has been made fully available and can be downloaded from the Dryad Data deposition.

For manuscripts utilizing custom algorithms or software that are central to the research but not yet described in published literature, software must be made available to editors and reviewers. We strongly encourage code deposition in a community repository (e.g. GitHub). See the Nature Portfolio guidelines for submitting code & software for further information.

Data

Policy information about availability of data

All manuscripts must include a data availability statement. This statement should provide the following information, where applicable:

- Accession codes, unique identifiers, or web links for publicly available datasets
- A description of any restrictions on data availability
- For clinical datasets or third party data, please ensure that the statement adheres to our policy

All analyses were conducted using publicly available datasets from UniProt (release 2018_11), the Marine Microbial Eukaryote Transcriptome Sequencing project (MMETSP0224, MMETSP0227, MMETSP0228, MMETSP0790), GenBank (e.g., SRR3221671 and various assemblies), or from individual manuscripts. All data sources are listed and available from the Dryad Data deposition.

Field-specific reporting

Please select the one below that is the best fit for your research. If you are not sure, read the appropriate sections before making your selection.

☐ Life sciences ☐ Behavioural & social sciences ☒ Ecological, evolutionary & environmental sciences

For a reference copy of the document with all sections, see nature.com/documents/nr-reporting-summary-flat.pdf

Ecological, evolutionary & environmental sciences study design

All studies must disclose on these points even when the disclosure is negative.

Study description	The study involved the systematic detection of horizontal gene transfer events across eukaryotic and viral genomes. High quality eukaryotic genomes from diverse taxa were selected and all viral genomes and NCLDV metagenomes with low contamination were also analyzed.
Research sample	All genomic data were obtained from UniProt (release 2018_11), the Marine Microbial Eukaryote Transcriptome Sequencing project (MMETSP0224, MMETSP0227, MMETSP0228, MMETSP0790), GenBank (e.g., SRR3221671 and various assemblies), or individual manuscripts. The accessions and sources for all datasets are listed in the Dryad data deposition.
Sampling strategy	Sample sizes (i.e., the number of genomic datasets used) were set such that good taxonomic coverage could be achieved while avoiding oversampling of individual eukaryotic groups and ensuring the computational feasibility of the analysis. For viral taxa, all genomic datasets estimated to have low contamination were used.
Data collection	Data were downloaded and stored by the corresponding author on a computer.
Timing and spatial scale	All data were downloaded within a month. The datasets were from representative species from across the tree of life. The representative nature and availability of these data does not change over time making the timing scale for data collection unimportant.
Data exclusions	No data were excluded in the analyses.
Reproducibility	The analysis can be reproduced using the files and code available from the Dryad data deposition.
Randomization	Samples/organisms were not allocated into groups making randomization unnecessary.
Blinding	Samples/organisms were not allocated into groups making blinding unnecessary.

Did the study involve field work? ☐ Yes ☒ No

Reporting for specific materials, systems and methods

We require information from authors about some types of materials, experimental systems and methods used in many studies. Here, indicate whether each material, system or method listed is relevant to your study. If you are not sure if a list item applies to your research, read the appropriate section before selecting a response.

Materials & experimental systems

n/a	Involved in the study
☒	☐ Antibodies
☒	☐ Eukaryotic cell lines
☒	☐ Palaeontology and archaeology
☒	☐ Animals and other organisms
☒	☐ Human research participants
☒	☐ Clinical data
☒	☐ Dual use research of concern

Methods

n/a	Involved in the study
☒	☐ ChIP-seq
☒	☐ Flow cytometry
☒	☐ MRI-based neuroimaging